OFFICE OF CIVILIAN RADIOACTIVE WASTE MANAGEMENT
ANALYSIS/MODEL COVER SHEET

QA: QA

Page: 1 of: 68 3/21/00

Complete Only Applicable Items

2. ☐ Analysis — Check all that apply	3. ☒ Model — Check all that apply
Type of Analysis: ☐ Engineering ☐ Performance Assessment ☐ Scientific	Type of Model: ☐ Conceptual Model ☐ Abstraction Model ☐ Mathematical Model ☐ System Model ☒ Process Model
Intended Use of Analysis: ☐ Input to Calculation ☐ Input to another Analysis or Model ☐ Input to Technical Document	Intended Use of Model: ☐ Input to Calculation ☒ Input to another Model or Analysis ☒ Input to Technical Document
Describe use:	Describe use:

4. Title:

Degradation of Stainless Steel Structural Material

5. Document Identifier (including Rev. No. and Change No., if applicable):

ANL-EBS-MD-000007 REV 00

6. Total Attachments:	7. Attachment Numbers - No. of Pages in Each:
N/A	N/A

	Printed Name	Signature	Date
8. Originator	Joseph C. Farmer R. Daniel McCright	Signature	Date 3/20/00
9. Checker	Denny Jones	David Stahl for Denny Jones	3/21/00
10. Lead/Supervisor	Al Lingenfelter	Al Lingenfelter	3/20/00
11. Responsible Manager	David Stahl	David Stahl	3/21/00

12. Remarks:

The designated originator and lead author of this AMR is Joseph Farmer. Contributing authors and researchers include Venkataraman Pasupathi, Daniel McCright, Joann Horn, Tiangan Lian, Peter Bedrossian, Francis Wang, John Estill, Ken King, Steve Gordon, Larry Logorette, Beverly Lum and David Fix. Technical comments by Joon Lee, Kevin Mon and members of the NWTRB are gratefully acknowledged. Data tracking was coordinated by Michael Coatsworth and Tom Gibson, and the lead editor was Kim Herrmann. QA comments by Charlie Warren and Richard Powe are appreciated. Direct management and oversight included George Dials, Dan Wilkins, Jean Younker, Mike Lugo, Hugh Benton, David Stahl, Martha Kohler, and Al Lingenfelter. Work was sponsored by the U.S. Department of Energy Office of Civilian and Radioactive Waste Management (OCRWM). This work was done under the auspices of the U.S. Department of Energy (DOE) by Lawrence Livermore National Laboratory (LLNL) under Contract No. W-7405-Eng-48.

OFFICE OF CIVILIAN RADIOACTIVE WASTE MANAGEMENT
ANALYSIS/MODEL REVISION RECORD

Complete Only Applicable Items

2. Analysis or Model Title:

Degradation of Stainless Steel Structural Material

3. Document Identifier (including Rev. No. and Change No., if applicable):

ANL-EBS-MD-000007 REV 00

4. Revision/Change No.	5. Description of Revision/Change
00	Initial issue

CONTENTS

Page

CONTENTS (Continued)

Page

FIGURES

Page

TABLES

Page

ABBREVIATIONS AND ACRONYMS

AFM	atomic force microscope or microscopy
AMR	analyses and models report
APC	aqueous phase corrosion
ASTM	American Society for Testing and Materials
CLST	container life and source term
CP	cyclic polarization
CRWMS	Civilian Radioactive Waste Management System
DOE	U.S. Department of Energy
DOX	dry oxidation
DS	drip shield
DTN	data tracking number
DWA	prefix for qualified Alloy 22 weight loss samples used in LTCTF
EBS	engineered barrier system
EDA	engineering design alternative
GC	general corrosion
HAC	humid air corrosion
HIC	hydrogen induced cracking
IRSR	issue resolution status report
KTI	key technical issue
LC	localized corrosion
LLNL	Lawrence Livermore National Laboratory
LTCTF	Long Term Corrosion Test Facility
M&O	Management and Operating Contractor
MIC	microbial influenced corrosion
NFE	near field environment
NRC	U.S. Nuclear Regulatory Commission
OCRWM	Office of Civilian Radioactive Waste Management
PMR	process model report
QA	quality assurance
RH	relative humidity

ABBREVIATIONS AND ACRONYMS (Continued)

SAW	simulated acidic concentrated water
SCC	stress corrosion cracking
SCE	saturated calomel electrode
SCW	simulated concentrated water
SDW	simulated dilute water
SEM	scanning electron microscopy
SIMS	secondary ion mass spectrometry
SIP	scientific investigation plan
SN	scientific notebook
SSW	simulated saturated water
TBV	to be verified
TDP	technical development plan
TEM	transmission electron microscopy
WAPDEG	waste package degradation code
WF	waste form
WP	waste package
WPOB	waste package outer barrier
wt.%	weight percent
XPS	X-ray photoelectron spectroscopy
XRD	X-ray diffraction
YMP	Yucca Mountain Project

1. PURPOSE

1.1 ANALYSES AND MODELS REPORT

As described in the *Monitored Geologic Repository Project Description Document* (CRWMS M&O 1999a), the recommended waste package (WP) design is a double-walled WP underneath a protective drip shield (DS). The purpose of the process-level model is to account for both general and localized corrosion of the WP structural support, which is assumed to be 316NG stainless steel. In regard to general and localized corrosion, 316L stainless steel is assumed to be an appropriate analog for 316NG. No 316NG stainless steel was available for testing. The model includes several sub-models, which account for dry oxidation (DOX), humid air corrosion (HAC), general corrosion (GC) in the aqueous phase, and localized corrosion (LC) in the aqueous phase. This analyses and models report (AMR) serves as a feed to the Waste Package Degradation (WAPDEG) analyses. It also serves as a basis for the WP process model report (PMR) and model abstraction for WAPDEG (CRWMS M&O 1999b).

1.2 BACKGROUND ON STAINLESS STEEL 316L

Alloy 22 is used as the corrosion resistant waste package outer barrier (WPOB). Stainless steel 316NG is to be used for construction of the structural support underneath the WPOB. The 316NG inner cylinder will increase the overall strength of the WP. Stainless steel 316L [UNS S31603] is considered to be a good analog for 316NG and has a composition of 16-18% Cr, 10-14% Ni, 2-3% Mo, 2% Mn (max.), 1% Si (max.), 0.03% C (max.), 0.045% P (max.), 0.03% S (max.), 0.10% N (max.), and Fe (balance) (CRWMS M&O 1999e, p. 13). This material is less susceptible to LC in environments that contain Cl^- than stainless steel 304 but more susceptible than other corrosion resistant materials (CRMs) such as Alloys 22, 625, and 825 that have been considered in various WP designs. The superior LC resistance of stainless steel 316L in comparison to 304 is apparently due to the addition of Mo, which is believed to help stabilize the passive film at low pH (Hack 1983). Molybdenum oxide is very insoluble at low pH (Pourbaix 1974). Consequently, 316L exhibits relatively high thresholds for localized attack.

1.3 ENVIRONMENT

The WP will experience a wide range of conditions during its service life. Initially, the high-level WPs will be hot and dry due to the heat generated by radioactive decay. However, the temperature will eventually drop to levels where both HAC and aqueous phase corrosion (APC) will be possible. Crevices will be formed between WP and supports; beneath mineral precipitates, corrosion products, dust, rocks, cement and biofilms; and between the Alloy 22 WPOB and the 316NG structural support. There has been concern that the crevice environment may be more severe than the near field environment (NFE). The hydrolysis of dissolved metal can lead to the accumulation of H^+ and a corresponding decrease in pH. Field-driven electromigration of Cl^- (and other anions) into the crevice must occur to balance cationic charge associated with H^+ ions (Gartland 1997; Walton et al. 1996). These exacerbated conditions can set the stage for the subsequent attack of WP materials by passive corrosion/dissolution, pitting, stress corrosion cracking (SCC), and hydrogen induced cracking (HIC). Passive corrosion implies very slow dissolution through a stable passive film. The passive corrosion rate is that

which corresponds to the passive current density. LC, SCC and HIC may also occur outside the crevice.

Such tests have been conducted in the Yucca Mountain Project's (YMP's) Long Term Corrosion Test Facility (LTCTF) (Estill 1998). Test media used in this facility include simulated acidic concentrated water (SAW), which is about one-thousand times (×1000) more concentrated than the ground water at Yucca Mountain (J-13 well water) and has been acidified with H_2SO_4 (Gdowski, UCRL-ID-132287). The measured pH of SAW is approximately 2.7.

1.4 RELATIONSHIP TO PRINCIPAL FACTORS

Degradation of the WP is key to understanding one of the most important principal factors in repository performance. This principal factor is the amount of water transmitted into and the rate of release of radionuclides out of the WP. The models and supporting experimental data to account for WP degradation, as well as the evolution of water involved in the various degradation processes, have been explored by Waste Package Operations (WPO). These models and supporting experimental data are reported in two separate PMRs, one for the WP and another for the waste form (WF). This AMR addresses the development of realistic models to account for the degradation of the 316NG stainless steel structural support inside the WPOB. Published data and data generated by YMP are used. This AMR is an integral part of the WP PMR, which also includes analyses for degradation of the WPOB and the DS. The WPOB will be fabricated from Alloy 22, and the DS will be fabricated from Ti Grade 7.

1.5 ACTIVITY PLANS

Approved activity plans and technical development plans were used in the performance of the work described in this document. Any necessary deviations from these activity plans are documented in the corresponding scientific notebooks (SNs). These procedures are compliant to the Office of Civilian Radioactive Waste Management (OCRWM) quality assurance (QA) requirements.

1.6 SUMMARY OF MODEL

The model for the general and LC of stainless steel 316NG (or 316L) is summarized in Figure 1. First, any corrosion of the structural support requires penetration of the WPOB. The threshold RH represented by Figure 2 and Equation 1 is first used to determine whether or not DOX will take place. If DOX is determined to occur, the parabolic growth law represented by Equations 6 through 12 is then used to calculate the corrosion rate as a function of temperature. If the threshold RH is exceeded, HAC will occur in the absence of dripping water, and APC will occur in the presence of dripping water. If APC is assumed to occur, the corrosion and critical potentials are used to determine whether the mode of attack is general or localized. The correlation represented by Equation 16 and Table 4 are used as the basis for estimating these potentials at the 50^{th} percentile. Since the material specifications will be based partly on the measured corrosion and critical potentials, it will be assumed that these potentials will be uniformly distributed about the 50^{th} percentile values determined from the correlation. For example, the 0^{th} and 100^{th} percentile values of E_{corr} will be assumed to be at E_{corr} (50^{th} percentile) $\pm \Delta E_{corr}$. Similarly, the 0^{th} and 100^{th} percentile values of $E_{critical}$ will be assumed to be at $E_{critical}$

(50^{th} percentile) ± $\Delta E_{critical}$. The desired values for ΔE_{corr} and $\Delta E_{critical}$ can be determined by inspecting Table 5. Values ranging from 24 to 75 mV seem like reasonable choices, based upon simulated saturated water (SSW). Materials would be tested before use, with any materials falling outside of the specified range being rejected. Acceptability is defined as a condition where no LC occurs. If the comparison of E_{corr} to $E_{critical}$ indicates GC, the distribution of rates determined from Figures 11 and 12 will be used as the basis of the general and localized rates of corrosion. This model does not yet account for the effects of aging and sensitization on corrosion rates. However, such enhancements of the corrosion rate will be accounted for in the future. Rates will be augmented to account for aging and MIC, as discussed in Sections 6.8 and 6.9.

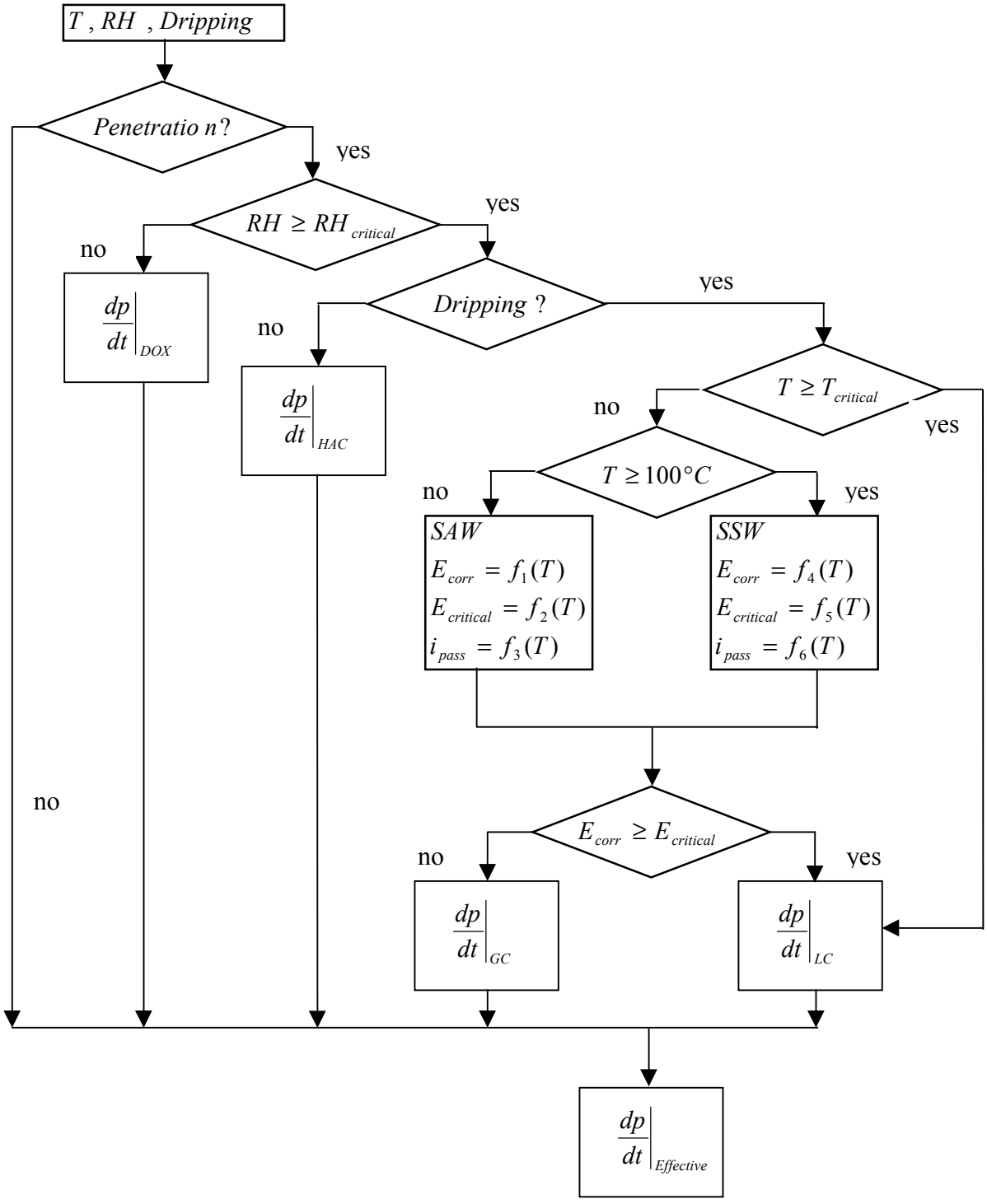

Figure 1. Schematic of Corrosion Model for Stainless Steel 316NG Structural Support

1.7 UNCERTAINTY AND VARIABILITY

The primary uncertainty in the threshold RH for HAC and APC is due to the presence of nitrate. Values of the equilibrium RH as a function of temperature for a saturated solution of $NaNO_3$ are given in Table 9 and Figure 8 of the AMR on WP surface environment (CRWMS M&O 2000a). Despite significant experimental work at Lawrence Livermore National Laboratory (LLNL), there continues to be significant uncertainty in the threshold RH for HAC and APC.

In an ideal case, the crevice corrosion temperature can be estimated from the intersection of the lines representing the corrosion and threshold potentials at elevated temperature. To force crevice corrosion to occur in the model, E_{corr} and $E_{critical}$ can simply be equated over temperature ranges of uncertainty. It is assumed that the crevice corrosion temperature is uniformly distributed over this range of uncertainty. Alternatively, the published data summarized in Figures 9 and 10 can be used to estimate critical temperatures.

Published rates of GC and LC are summarized in Tables 6 through 9, as well as in Figures 11 through 14. From comparing the data for 304 and 316 stainless steels, the advantages of molybdenum additions are evident. The corrosion rates of 304 are higher than comparable rates of 316. Type 316 stainless steel contains more molybdenum than Type 304 stainless steel. From Figure 12, the LC rates of 316 appear to lie between 10^3 and 10^4 μm y^{-1}. The GC rates for APC of 316 appear to lie between 10^{-1} and 10^2 μm y^{-1}. The GC rates for HAC (atmospheric corrosion) of 316 appear to lie between 10^{-3} and 10^{-1} μm y^{-1}. It is assumed that the published rates for 316 are representative of those for 316NG. The regression line shown in Figure 12 is assumed to represent both uncertainty and variability.

1.8 RESOLUTION OF COMMENTS IN ISSUE RESOLUTION STATUS REPORT

The issue resolution status report (IRSR) recently issued by the NRC (1999) provides guidance for the development of process-level models. The primary consideration in the key technical issue (KTI) is the container life and source term (CLST). There must be a high degree of confidence in the adequacy of the engineered barrier system (EBS) design, thereby providing assurance that containers will be adequately long-lived, and radionuclide releases from the EBS will be sufficiently controlled. The container design and the packaging of spent nuclear fuel (SNF) and high-level waste (HLW) glass are expected to make a significant contribution to the overall repository performance. The IRSR defines the physical boundary of the EBS by the walls of the WP emplacement drifts. The IRSR deems six sub-issues to be important to the resolution of the KTI. The first sub-issue is specifically relevant to this AMR: the effects of corrosion processes on the lifetime of the containers.

The acceptance criteria for sub-issue 1 are:

1. DOE has identified and considered likely modes of corrosion for container materials, including dry-air oxidation, humid-air corrosion, and aqueous corrosion processes, such as GC, LC, MIC, SCC and HIC, as well as the effect of galvanic coupling.

Response: This AMR includes process-level models for DOX, HAC, and APC processes, such as GC, LC, and MIC. Galvanic coupling effects have been minimized to the extent possible and will be accounted for in greater detail in future revisions. Both SCC and HIC are dealt with in companion AMRs.

2. DOE has identified the broad range of environmental conditions within the WP emplacement drifts that may promote the corrosion processes listed previously, taking into account the possibility of irregular wet and dry cycles that may enhance the rate of container degradation.

   Response: This AMR includes environmental thresholds that can be used to switch between dominant modes of corrosion. For example, as the WP temperature drops and the RH increases, the mode of attack changes from dry-air oxidation to humid-air or aqueous-phase corrosion. A comparison of the corrosion and threshold potentials is used to determine whether or not LC will occur.

3. DOE has demonstrated that the numerical corrosion models used are adequate representations, taking into consideration associated uncertainties, of the expected long-term behaviors and are not likely to underestimate the actual degradation of the containers as a result of corrosion in the repository environment.

   Response: Uncertainties are accounted for in corrosion rates. Published rates of GC and LC are summarized in Tables 6 through 9, as well as in Figures 11 through 14. From comparing the data for 304 and 316 stainless steels, the advantages of molybdenum additions are evident. The corrosion rates of 304 are higher than comparable rates of 316. Type 316 stainless steel contains more molybdenum than Type 304 stainless steel. From Figure 12, the LC rates of 316 appear to lie between 10^{3} and 10^{4} $\mu m\ y^{-1}$. The GC rates for APC of 316 appear to lie between 10^{-1} and 10^{2} $\mu m\ y^{-1}$. The GC rates for HAC (atmospheric corrosion) of 316 appear to lie between 10^{-3} and 10^{-1} $\mu m\ y^{-1}$. It is assumed that the published rates for 316 are representative of those for 316NG. The regression line shown in Figure 12 is assumed to represent both uncertainty and variability.

4. DOE has considered the compatibility of container materials, the range of material conditions, and the variability in container fabrication processes, including welding, in assessing the performance expected in the containers intended waste isolation.

   Response: The effects of welding and thermal aging on the corrosion resistance of the WP materials will be accounted for as discussed in Sections 5.7 and 6.8, both entitled *Effect of Thermal Aging and Sensitization on Corrosion*. In published aging studies conducted with Type 316 stainless steel at 816°C for up to 10,000 hours, the $M_{23}C_6$ concentration increases almost immediately. The chi (χ) phase begins to precipitate at about 150 hours, while the sigma (σ) and Laves phases do not begin to precipitate until about 500 and 1000 hours, respectively. By lowering the carbon content of Type 316 stainless steel to a level corresponding to Type 316L, the time required for formation of a given quantity of $M_{23}C_6$ is significantly lengthened. After the precipitated carbide phase reaches a maximum, it can begin to redissolve into the bulk. The formation of both $M_{23}C_6$ and sigma phases are accelerated by cold working.

Sensitization is a term denoting increased susceptibility to attack following a thermal exposure that causes chromium-rich $M_{23}C_6$ carbides to precipitate at grain boundaries. The subject of sensitization has been the subject of extensive investigation. Chromium carbide precipitation in stainless steels occurs in the temperature range from 500 to 850°C (930 to 1560°F) with the rate of precipitation controlled by chromium diffusion. A variety of metallurgical changes have been suggested as mechanisms for sensitization, but it is generally accepted that the principal feature responsible is a narrow chromium-depleted zone adjacent to the carbides. It is generally accepted that susceptibility to intergranular attack occurs when there is an essentially continuous zone in which the local chromium concentration is below about 13 atomic percent. Chromium is the element responsible for the formation of stable passive films on stainless steels, and localized depletion of this element adjacent to grain boundaries results in the establishment of an active path (one which does not readily repassivate) into the bulk material. The width of this chromium-depleted region is typically 200 nm. The effect of thermal aging on the corrosion rate is accounted for in an enhancement factor for sensitized grain boundaries (G_{aged}). In the case of non-sensitized base metal, this enhancement factor is unity ($G_{aged} \sim 1$), whereas the value for completely sensitized grain boundary is much larger ($G_{aged} \sim 10$). Material with less carbide precipitation than the fully sensitized material would have an intermediate value of G_{aged} ($1 \leq G_{aged} \leq 10$). Here it is assumed that these depleted regions are about 200 nm wide ($\delta = 2\times10^{-5}$ cm). The fraction falling within the chromium-depleted region would experience corrosion rate enhancement ($G_{aged} \geq 1$). Alternatively, LC rates could be applied to the fraction of the area represented by θ_{GB}, with GC rates applied to the remaining area.

5. DOE has justified the use of data collected in corrosion tests not specifically designed or performed for the Yucca Mountain repository program for the environmental conditions expected to prevail at the YM site.

   Response: The threshold RH used to determine whether vapor phase attack is by DOX or HAC is based upon the deliquescence point of salt deposits that could form on the WP surface due to aerosol transport. Measurements of GC rates in the vapor and aqueous phases, electrochemical potentials, and other relevant performance data were in test media that can be directly related to water chemistry expected on the WP surface during the service life of Alloy 22. These water chemistries are based upon evaporative concentrations of the standard J-13 well water chemistry. Crevice chemistry is being measured in situ, with and without the presence of buffer ions. In the aqueous phase, a range of temperature extending from room temperature to 120°C is being investigated. The high-temperature limit is based upon the boiling point of a near-saturation water chemistry without buffer. The expected boiling point of the aqueous phase on the WP surface is expected to be lower.

6. DOE has conducted a consistent, sufficient, and suitable corrosion testing program at the time of the LA submittal. In addition, DOE has identified specific plans for further testing to reduce any significant area(s) of uncertainty as part of the performance confirmation program.

Response: The DOE has established a corrosion test program that addresses all anticipated modes of corrosive attack of the WP. Studies include exposure of over 18,000 samples of candidate WP material in the LTCTF. A large number of pre- and post-exposure measurements of dimension and weight allow establishment of distribution functions for representation of the GC rate. Microscopic examination of samples from the LTCTF and other corrosion tests is done with scanning electron microscopy (SEM), atomic force microscopy (AFM), X-ray diffraction (XRD), X-ray photoelectron spectroscopy (XPS), secondary ion mass spectrometry (SIMS), and other state-of-the-art surface analytical techniques. Potentiodynamic and potentiostatic electrochemical tests are conducted with base metal, thermally aged material, and simulated welds. Thermally aged material is fully characterized with the transmission electron microscope (TEM) as discussed by Summers (CRWMS M&O 2000b).

7. DOE has established a defensible program of corrosion monitoring and testing of the engineered subsystems components during the performance confirmation period to assure they are functioning as intended and anticipated.

   Response: The DOE has established a corrosion test program that addresses all anticipated modes of corrosive attack of the WP. There is a clear linkage between the experimental data being collected and modules in the predictive WAPDEG code that serves as the heart of the Total System Performance Assessment (TSPA). Data and modules have been developed for each key element of the EDA II design: the WPOB (Alloy 22), the inner structural support (stainless steel 316NG), and the protective DS (Ti Grade 7). Companion AMRs provide data and modules for the stainless steel 316NG and the Ti Grade 7 alloy.

2. QUALITY ASSURANCE

The Quality Assurance (QA) program applies to this analysis. All types of WPs were classified (per QAP-2-3) as Quality Level-1. CRWMS M&O (1999c, p. 7) in *Classification of the MGR Uncanistered Spent Nuclear Fuel Disposal Container System* is cited as an example of a WP type. The development of this analysis is conducted under activity evaluation *11017040 Long Term Materials Testing and Modeling* (CRWMS M&O 1999d), which was prepared per QAP-2-0. The results of that evaluation were that the activity is subject to the *Quality Assurance Requirements and Description* (DOE 2000) requirements.

3. COMPUTER SOFTWARE AND MODEL USAGE

3.1 SOFTWARE ROUTINES

The electronic notebook discussed in AP-E-20-81 was kept with Microsoft Excel 97. Calculations used to manipulate raw data were performed electronically in spreadsheets created with Microsoft Excel 97. The Microsoft Excel 97 that was used was bundled with Microsoft Office 97 Professional Edition for Windows 95/NT or Workstation 4.0 (SN # 269-056-174). Excel is considered exempt from the OCRWM procedure entitled *Software Configuration Management* (AP-SI.1Q).

The correlation equations presented in this document were created within Excel spreadsheets. Those correlation equations were checked by hand calculation, using a Hewlett-Packard 20S scientific calculator. All correlation equations were found to be reasonable predictors of the represented data. Many of the tabulated calculations were also checked by hand calculation.

3.2 INTEGRITY OF TRANSFER OF DATA

The integrity of electronic data transfer has been verified as required by OCRWM Procedure YAP-SV.1Q. The comparison method was used to ensure the accuracy of the transferred data. A sampling of approximately 5% of the data in the source file was visually compared to the corresponding data in the transferred file. The data selected was at the reviewer's discretion. Reviewers included the originator as well as the document editor and QA staff.

4. INPUTS

4.1 DATA AND PARAMETERS

4.1.1 Definition of Parameters

b_0	coefficient in regression equation
b_1	coefficient in regression equation
b_2	coefficient in regression equation
i_{corr}	corrosion current density
i_{pass}	passive current density
k	parabolic rate constant in DOX model
p	wall penetration due to corrosive attack
t	exposure time during weight loss measurement
t	time in DOX model
w_{oxide}	formula weight of oxide formed during DOX
x	independent variable in regression equation
x	oxide thickness in DOX model
y	dependent variable in regression equation
z_i	valence (charge) of the i^{th} ion
D_{oxide}	diffusivity of reacting species through protective oxide
E_{corr}	corrosion potential
$E_{critical}$	critical potential – threshold for localized attack
E_j	junction potential
J_{oxide}	flux of reacting species through protective oxide
R	universal gas constant
R^2	regression coefficient
RH	relative humidity
$RH_{critical}$	threshold RH for HAC
T	temperature
σ	standard deviation

μ	mean
ρ	density of Stainless steel 316L
ρ_{oxide}	density of oxide formed during DOX
ζ_{oxide}	stoichiometric coefficient for DOX reaction

4.1.2 Determination of Input Parameters

Input for this AMR includes bounding conditions for the local environment on the WP surface, which include temperature, relative humidity (RH), presence of liquid-phase water, liquid-phase electrolyte concentration (chloride, buffer, and pH), and oxidant level. The detailed evolution of the environment on the WP surface is defined by a companion AMR entitled *Environment on the Surface of Drip Shield and Waste Package Outer Barrier* (CRWMS M&O 2000a). This work has been used to define the threshold RH for HAC and APC as well as a medium for testing WP materials under what is now believed to be a worst-case scenario. This test medium is referred to here as SSW and has a boiling point of approximately 120°C.

As discussed in CRWMS M&O (2000a), the AMR on WP environment, hygroscopic salts may be deposited by aerosols and dust introduced with the backfill. They will be dissolved in seepage water that enters the drifts and the episodic water that flows through the drifts. Salts will be deposited on the WP surface during evaporation. Such hygroscopic salts, deposited on WP surfaces, enable aqueous solutions to exist as thin surface films at relative humidities below 100%. The threshold RH ($RH_{critical}$) at which a thin-film aqueous solution can exist on the surface is defined as the deliquescence point (CRWMS M&O 2000a). This threshold defines the condition necessary for aqueous electrochemical corrosion processes of a metal with salt deposits to occur at a given temperature. It is believed that evaporation will produce a solution with sodium, potassium, chloride, and nitrate ions. Other ions may be present but at significantly lower levels. The deliquescence point of NaCl is relatively constant with temperature and varies from 72-75%. In contrast, the deliquescence point of $NaNO_3$ has a strong dependence on temperature, ranging from an *RH* of 75.36% at 20°C to 65% at 90°C. The implied equilibrium *RH* is 50.1% at 120.6°C. The primary uncertainty in the threshold *RH* for HAC and APC is due to the presence of nitrate. Values of the equilibrium *RH* as a function of temperature for a saturated solution of $NaNO_3$ are given in Table 8 and Figure 8 of the AMR on WP surface environment (CRWMS M&O 2000a). It is assumed that any other salts with lower deliquescence points ($RH_{critical}$) are precipitated. For the time being, this threshold will be assumed to obey the following polynomial in temperature, which is a fit of the data deliquescence point data for $NaNO_3$:

$$RH_{critical} = -3.5932\times10^{-5}\times T(°C)^3 + 5.9649\times10^{-3}\times T(°C)^2 - 0.45377\times T(°C) + 81.701 \quad \text{(Eq. 1)}$$

$R^2 = 0.9854$,

where R^2 is the coefficient of determination and where R is the coefficient of correlation. This correlation is compared to the data in Figure 2 below.

As discussed in Section 6.5.2 of the AMR on DS and WP environment (CRWMS M&O 2000a), the evaporative concentration of J-13 well water results in the concentration of Na^+, K^+, Cl^-, and

NO_3^-. The concentration of HCO_3^- reaches a constant level, while the concentrations of F^- and SO_4^{2-} initially increase but eventually fall due to precipitation. Ultimately, the F^- drops below the level of detection. The SSW formulation is based upon the assumption that evaporation of J-13 eventually leads to a sodium-potassium-chloride-nitrate solution. The absence of sulfate and carbonate in this test medium is believed to be conservative, in that carbonate would help buffer pH in any occluded geometry such as a crevice. Polyprotic anions with multistep dissociation tend to serve as buffers.

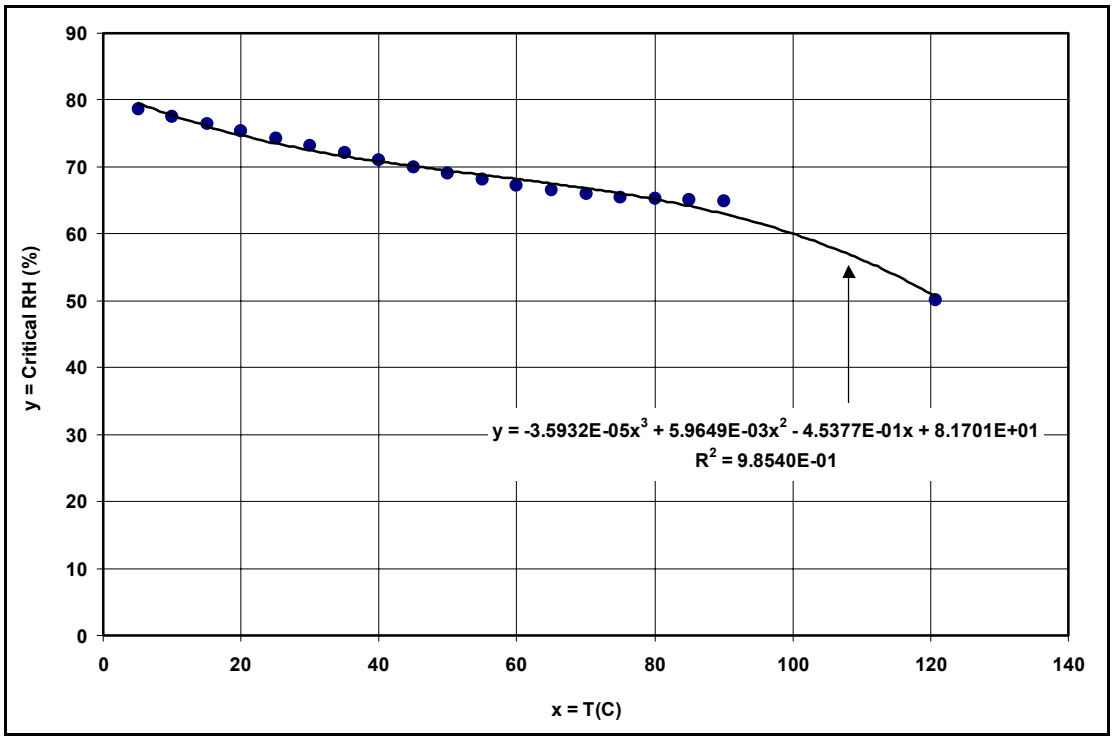

DTN: LL991208205924.096

Figure 2. Deliquescence Point for Sodium Nitrate Solutions

As pointed out in CRWMS M&O (2000a), the deliquescence point can cover a broad range. For example, the deliquescence point of NaOH is 1.63% at 75°C. The deliquescence point of K_2SO_4 is 97.59% at 20°C. It is assumed that the uncertainty in $RH_{critical}$ can be represented by a triangular distribution (Section 6.5.4). The value at the 50th percentile is represented by Equation 1. Values at the 0th and 100th percentiles are assumed to be 0 and 100%, respectively.

4.2 CRITERIA

The following criterion applies to general corrosion and localized corrosion of the WPOB of all WP designs (CRWMS M&O 1999f).

The disposal container/WP shall be designed, in conjunction with the Emplacement Drift System and the natural barrier, such that the expected annual dose to the average member of the critical group shall not exceed 25 mrem total effective dose equivalent at any time during the first

10,000 years after permanent closure, as a result of radioactive materials released from the geologic repository (CRWMS M&O 1999f) (Section 1.2.1.3).

4.3 CODES AND STANDARDS

4.3.1 Standard Test Media

G. E. Gdowski, Formulation and Make-up of Simulated Acidic Concentrated Water (SAW), High Ionic Content Aqueous Solution, Yucca Mountain Project, Lawrence Livermore National Laboratory, Livermore, CA, TIP-CM-08, Revision CN TIP-CM-08-0-2, April 4, 1997, Table 1, p. 3. UCRL-ID-132287.

G. E. Gdowski, Formulation and Make-up of Simulated Dilute Water (SDW), Low Ionic Content Aqueous Solution, Yucca Mountain Project, Lawrence Livermore National Laboratory, Livermore, CA, TIP-CM-06, Revision CN TIP-CM-06-0-2, April 4, 1997, Table 1, p. 3. UCRL-ID-132286.

G. E. Gdowski, Formulation and Make-up of Simulated Concentrated Water (SCW), High Ionic Content Aqueous Solution, Yucca Mountain Project, Lawrence Livermore National Laboratory, Livermore, CA, TIP-CM-07, Revision CN TIP-CM-07-0-2, April 4, 1997, Table 1, pp. 3–4. UCRL-ID-132285.

4.3.2 General Corrosion Measurements

Standard Practice for Preparing, Cleaning, and Evaluating Corrosion Test Specimens, Designation G 1-90, 1997 Annual Book of American Society for Testing and Materials (ASTM) Standards, Section 3, Vol. 3.02, pp. 15–21.

Standard Practice for Preparing, Cleaning, and Evaluating Corrosion Test Specimens, Designation G 1-81, 1987 Annual Book of ASTM Standards, Section 3, Vol. 3.02, pp. 89–94, Subsection 8 – Calculation of Corrosion Rate, Appendix X1 – Densities for a Variety of Metals and Alloys.

ASTM G48-99a. 1999. *Standard Test Methods for Pitting and Crevice Corrosion Resistance of Stainless Steels and Related Alloys by Use of Ferric Chloride Solution.* West Conshohocken, Pennsylvania: American Society for Testing and Materials.

4.3.3 Cyclic Polarization Measurements

Standard Reference Test Method for Making Potentiostatic and Potentiodynamic Anodic Polarization Measurements, Designation G 5-87, 1989 Annual Book of ASTM Standards, Section 3, Vol. 3.02, pp. 79-85.

Standard Practice for Conventions Applicable to Electrochemical Measurements in Corrosion Testing, Designation G 3-89, 1997 Annual Book of American Society for Testing and Materials (ASTM) Standards, Section 3, Vol. 3.02, pp. 36–44.

Standard Test Method for conducting Cyclic Potentiodynamic Polarization Measurements for Localized Corrosion Susceptibility of Iron-, Nickel-, or Cobalt-Based Alloys, Designation G 61-86, 1997 Annual Book of American Society for Testing and Materials (ASTM) Standards, Section 3, Vol. 3.02, pp. 231–235.

Standard Reference Test Method for Making Potentiostatic and Potentiodynamic Anodic Polarization Measurements, Designation G 5-94, 1997 Annual Book of American Society for Testing and Materials (ASTM) Standards, Section 3, Vol. 3.02, pp. 54–57.

5. ASSUMPTIONS

5.1 DRY OXIDATION

It is assumed first that the Alloy 22 WPOB must be penetrated before significant DOX of the inner 316L component can occur. Thereafter, DOX occurs at any RH below the threshold ($RH_{critical}$) for HAC:

$$RH < RH_{critical} \quad \text{(Eq. 2)}$$

$RH_{critical}$ is assumed to obey Equation 1. DOX forms an adherent, protective oxide film of uniform thickness. The rate of DOX will be assumed to be limited by mass transport through the growing metal oxide film. Consequently, the oxide thickness will obey either a logarithmic or parabolic growth law (film thickness proportional to the square root of time). Due to the availability of data to support the parabolic growth law, those kinetics are assumed here. Reasonable values of the parabolic rate constant will be assumed, as discussed in Section 6.1. DOX is assumed to occur uniformly over each WAPDEG patch, which is comparable in size to that of a LTCTF sample with generic weight-loss geometry. Welding is assumed to have no significant effect on the DOX threshold and rate. Backfill is also assumed to have no significant effect on the DOX threshold and rate. These assumptions are relevant to the analysis presented in Section 6.1.

As pointed out in CRWMS M&O (2000a), the deliquescence point can cover a broad range. For example, the deliquescence point of NaOH is 1.63% at 75°C. The deliquescence point of K_2SO_4 is 97.59% at 20°C. It is assumed that the uncertainty in $RH_{critical}$ can be represented by a triangular distribution (CRWMS M&O 2000d, Section 6.5.4, Attachment II). The value at the 50^{th} percentile is represented by Equation 1. Values at the 0^{th} and 100^{th} percentiles are assumed to be 1.63 and 97.59%, respectively.

5.2 HUMID AIR CORROSION

The WPOB must be penetrated before significant HAC can occur. After penetration of the WPOB, it is assumed that HAC occurs at any RH above the threshold, provided that there is no dripping or other episodic water intrusions:

$$RH \geq RH_{critical} \quad \text{(Eq. 3)}$$

This threshold RH for HAC ($RH_{critical}$) is assumed to obey Equation 1, which is taken from the AMR entitled *Environment on the Surface of Drip Shield and Waste Package Outer Barrier* (CRWMS M&O 2000a). As a bounding worst-case assumption based on a conservative approach, it will be assumed that the rate of HAC is identical to the largest observed rate for APC during the period where HAC is operable. It will also be assumed that the corrosion rate is constant, and does not decay with time. Therefore, the combined distributions presented here are based upon the combined data for the vapor and aqueous phases and are assumed to represent HAC and APC equally well. Less conservative corrosion models assume that the rate decays with time. HAC is assumed to occur uniformly over each WAPDEG patch, which is comparable in size to that of a LTCTF sample with generic weight-loss geometry. Welding is assumed to have no significant effect on the HAC threshold and rate. Backfill is also assumed to have no significant effect on the HAC threshold and rate. These assumptions are relevant to the analysis presented in Section 6.2.

5.3 AQUEOUS PHASE CORROSION

The WPOB must be penetrated before significant APC of the underlying 316NG structural support can occur. After penetration of the WPOB, the existence of liquid-phase water on the WP depends upon the presence of a salt and mineral deposit. In the presence of such a deposit, a liquid-phase can be established at a higher temperature than otherwise possible. In the model discussed here, it is assumed that two conditions must be met for APC: dripping water and RH above the deliquescence point of the deposit at the temperature of the 316NG structural support.

$$RH \geq RH_{critical} \qquad \text{(Eq. 4)}$$

This threshold RH for HAC ($RH_{critical}$) is assumed to obey Equation 1, which is based upon the AMR entitled *Environment on the Surface of Drip Shield and Waste Package Outer Barrier* (CRWMS M&O 2000a). For the time being, the composition of the electrolyte formed on the WP surface is assumed to be that of SCW below 100°C and that of SSW above 100°C. It will be assumed that the corrosion rate is constant and does not decay with time. Less conservative corrosion models assume that the rate decays with time. General APC is assumed to occur uniformly over each WAPDEG patch, which is comparable in size to that of a LTCTF sample with generic weight-loss geometry. Welding is assumed to have no significant effect on the APC threshold and rate. Backfill is also assumed to have no significant effect on the APC threshold and rate. These assumptions are relevant to the analysis presented in Section 6.3.

5.4 THRESHOLD FOR LOCALIZED CORROSION

If the open circuit corrosion potential (E_{corr}) of the 316NG is less than the threshold potential for LC ($E_{critical}$), it will be assumed that no LC occurs.

$$E_{corr} < E_{critical} \qquad \text{(Eq. 5)}$$

Threshold values have been determined for 316L in various representative environments, as discussed in Section 6.4. Stainless steel 316L is assumed to be an adequate analog for 316NG. In an ideal case, the crevice corrosion temperature can be estimated from the intersection of the

lines representing the corrosion and threshold potentials at elevated temperature. To force crevice corrosion to occur in the model, E_{corr} and $E_{critical}$ can simply be equated over temperature ranges of uncertainty. It is assumed that the crevice corrosion temperature is uniformly distributed over this range of uncertainty. This assumption is relevant to the analysis presented in Section 6.4.3 and is based on a conservative approach for crevice corrosion temperature. Alternatively, the published data summarized in Figures 9 and 10 can be used to estimate critical temperatures.

5.5 EFFECT OF GAMMA RADIOLYSIS ON CORROSION POTENTIAL

The effects of oxidant can be accounted for through the open circuit corrosion potential (E_{corr}). Based upon published data described in Section 6.6, it is believed that the shift in corrosion potential due to gamma radiolysis will be significantly less than 200 mV.

5.6 EFFECT OF MICROBIAL GROWTH ON CORROSION POTENTIAL

The effect of microbial growth on E_{corr} and GC rates for 316L have been studied by LLNL (Horn et al. 1998; Lian et al. 1999). End-point measurements of E_{corr} in both inoculated and sterile media indicate that microbial growth does not have any large impact on this parameter. The GC rate appears to be doubled in the presence of microbes. More work is needed to help resolve this issue in the future. This assumption is relevant to the analyses presented in Sections 6.4, 6.5 and 6.8 and will be further developed in the future.

5.7 EFFECT OF THERMAL AGING AND SENSITIZATION ON CORROSION

First, it is assumed that the WP temperature is kept below 300°C. With this constraint, the impact of aging and phase instability on the corrosion of stainless steel 316NG is expected to be insignificant. This is based on the limited data available on Alloy 22 at this time.

5.8 ASSUMPTIONS PERTAINING TO INNER BARRIER

The stainless steel 316NG inner barrier of the WP provides structural integrity for the WP until the outer barrier fails. Thus far, there has been no intention to claim credit for the corrosion resistance of this stainless steel layer. This AMR provides a technical basis for claiming credit for the inner barrier in the event that the strategy changes.

After penetration of the WPOB, the formation of a crevice between the Alloy 22 and 316NG is possible. The formation of a low-pH crevice environment in this interfacial region is possible, as discussed in Section 6.7. Crevice corrosion of the Alloy 22 due to the local chemistry established through hydrolysis of dissolved metal from the 316NG could be severe. While such inside-out attack is not accounted for in the present model, it may be desirable to account for it in the future, especially in crevice regions with welds that might be susceptible to SCC.

6. ANALYSIS/MODEL

6.1 DRY OXIDATION

After penetration of the WPOB, it is assumed that DOX of the 316NG structural support will occur at any RH below the threshold for HAC.

$$RH < RH_{critical} \quad \text{(Eq. 6)}$$

This process is assumed to result in the formation of an adherent, protective oxide film (primarily Cr_2O_3) of uniform thickness. The oxidation reaction given as (Welsch et al. 1996; CRWMS M&O 2000d):

$$4/3\ Cr + O_2 \longrightarrow 2/3\ Cr_2O_3 \quad \text{(Eq. 7)}$$

The rate of dry oxidation will be assumed to be limited by mass transport through this growing metal oxide film. Fick's first law is applied, assuming a linear concentration gradient across the oxide film of thickness x:

$$J_{oxide} = -D_{oxide} \frac{\partial C}{\partial x} \approx -D_{oxde} \frac{\Delta C}{x} \quad \text{(Eq. 8)}$$

where J_{oxide} is the molar flux of the reacting species in the oxide, D_{oxide} is the diffusivity of the reacting species in the oxide, ΔC is the corresponding differential molar concentration. Oxide growth is related to the flux by:

$$\frac{dx}{dt} = \frac{\zeta_{oxide} \times w_{oxide} \times J_{oxide}}{\rho_{oxide}} \quad \text{(Eq. 9)}$$

where ζ_{oxide} is the stoichiometric coefficient (moles of oxide per mole of diffusing species), w_{oxide} is the formula weight of the oxide, and ρ_{oxide} is the density of the oxide. Integration shows that the oxide thickness should obey the following parabolic growth law (Welsch et al. 1996), also known as Wagner's Law, where the film thickness is proportional to the square root of time:

$$x = \sqrt{x_0^2 + k \times t} \quad \text{(Eq. 10)}$$

where x_0 is the initial oxide thickness, x is the oxide thickness at time t, and k is a temperature-dependent parabolic rate constant. More specifically, k is defined as follows:

$$k = \frac{2 \times \zeta_{oxide} \times w_{oxide} \times D_{oxide} \times \Delta C}{\rho_{oxide}} \quad \text{(Eq. 11)}$$

To facilitate an approximate calculation, published values of k can be used (Welsch et al. 1996). From Figure 18 of this reference, it is concluded that all observed values of k fall below a line defined by:

$$\log\left[k\left(m^2 s^{-1}\right)\right] = -12.5 \times \left(\frac{10^3}{T(K)}\right) - 3.5 \qquad \text{(Eq. 12)}$$

where T is defined as the absolute temperature. The highest temperature is expected to be approximately 350°C (623 K), which corresponds to the limit for the fuel cladding. The value of k corresponding to this upper limit is 2.73×10^{-24} m^2 s^{-1} (8.61×10^{-5} square microns per year). After one year, this corresponds to a growth of 0.0093 microns (about 9.3 nm per year). As will be seen in subsequent discussion, this estimated rate is comparable to that expected for APC at lower temperatures. It is therefore recommended that dry oxidation of the stainless steel 316NG or 316L be accounted for through application of the parabolic law. The above expression represents a conservative upper bound, based upon the published literature.

As discussed in the AMR for corrosion of the titanium DS (CRWMS M&O 2000c), logarithmic growth laws may be more appropriate at relatively lower temperature than parabolic laws. However, such logarithmic expressions predict that the oxide thickness (penetration) asymptotically approaches a small maximum level. In contrast, the parabilic law predicts continuous growth of the oxide, which is much more conservative. Since such conservative estimates of the dry oxidation rate do not appear to be life limiting and reliable data for determining the maximum oxide thickness on 316NG (or 316L) do not appear to be available, the parabolic growth law will be used for the 316NG structural support.

The DOX model presented here assumes uniform oxidation of the 316NG surface inside the penetrated WPOB. In the future, the possibility of preferential DOX along grain boundaries in the 316NG should be considered. This is a generic failure mode recognized by Dr. D. S. Dunn of the Southwest Research Institute in San Antonio, Texas in November 1999 in regard to Alloy 22. He is a representative of the U.S. Nuclear Regulatory Commission. Such preferential attack would ultimately be diffusion controlled, with the diffusion path being equivalent to the length of oxidized grain boundary.

6.2 HUMID AIR CORROSION

After penetration of the WPOB, it is assumed that HAC of the 316NG structural support will occur above a threshold RH, provided that there is no dripping:

$$RH \geq RH_{critical} \qquad \text{(Eq. 13)}$$

This threshold RH for HAC ($RH_{critical}$) is assumed to obey Equation 1, which is based upon the AMR entitled *Environment on the Surface of Drip Shield and Waste Package Outer Barrier* (CRWMS M&O 2000a). The existence of this threshold is due to the dependence of water adsorption on RH.

Despite significant experimental work, there continues to be significant uncertainty in the threshold RH for HAC and APC. Other salts are known to have deliquescence points below that of $NaNO_3$. Furthermore, it is known that two monolayers of water can exist on a metal surface at only 40% RH. The approximate number of water monolayers on typical metal surfaces as a function of RH is given by Leygraf (1995) and repeated below in Table 1.

Table 1. Coverage of Metal Surfaces by Water

Relative Humidity (%)	Number of Water Monolayers
20	1
40	1.5-2
60	2-5
80	5-10

It will be assumed that HAC can be treated as uniform GC. As a bounding worst-case assumption, it will be assumed that the rate of HAC can be represented by the atmospheric corrosion rates shown in Figures 12 and 13. It will also be assumed that the corrosion rate is constant and does not decay with time (Gdowski and Bullen 1988). As pointed out in CRWMS M&O (2000d), observed deliquescence points cover a very broad range of RH. The deliquescence point of NaOH is 1.63% RH at 75°C, while that of K_2SO_4 is 97.59% RH at 20°C. It is assumed that the uncertainty in $RH_{critical}$ can be represented by a triangular distribution. The triangular distribution is described in Section 6.5.4 of the companion AMR on the WPOB (CRWMS M&O 2000d). The value at the 50th percentile is represented by Equation 1. Values at the 0th and 100th percentiles are assumed to be 1.63 and 97.59%, respectively.

6.3 AQUEOUS PHASE CORROSION

After penetration of the WPOB and at a given surface temperature, the existence of liquid-phase water on the 316NG structural support depends upon the presence of a salt and mineral deposit. In the presence of such a deposit, a liquid-phase can be established at a higher temperature than otherwise possible. In the model discussed here, it is assumed that two conditions must be met for APC: dripping water; and RH above the deliquescence point of the deposit at the temperature of the 316NG structural support.

$$RH \geq RH_{critical} \qquad \text{(Eq. 14)}$$

This threshold RH for HAC ($RH_{critical}$) is assumed to obey Equation 1, which is based upon the AMR entitled *Environment on the Surface of Drip Shield and Waste Package Outer Barrier* (CRWMS M&O 2000a). For the time being, the composition of the electrolyte formed at the interface between the 316NG and the WPOB is assumed to be that of SCW below 100°C and that of SSW above 100°C. It will be assumed that the corrosion rate is constant and does not decay with time. Less conservative corrosion models assume that the rate decays with time.

6.4 LOCALIZED CORROSION

6.4.1 Threshold Potentials of Stainless steel 316L

The LC model for stainless steel 316NG (analogous to 316L) assumes that localized attack occurs if the open circuit corrosion potential (E_{corr}) exceeds the conservative threshold potential for possible breakdown of the passive film ($E_{critical}$):

$$E_{corr} \geq E_{critical} \quad \text{(Eq. 15)}$$

6.4.2 Cyclic Polarization in Synthetic Concentrated J-13 Well Waters

The YMP has used CP to determine threshold potentials for titanium alloys in various test media relevant to the environment expected in the repository. These test media are based upon J-13 well water chemistry (Harrar et al. 1990). Relevant test environments include simulated SDW, SCW, and SAW at 30, 60, and 90°C, as well as SSW at 100 and 120°C. The compositions of these test media are based upon the work at LLNL (Gdowski, UCRL-ID-132287; UCRL-ID-132286; UCRL-ID-132285). The SSW composition has been recently developed (CRWMS M&O 2000a) and is documented in a companion AMR on GC and LC of the WPOB (CRWMS M&O 2000d). These test media are summarized in Table 2 below. In general, anions such as chloride promote LC; whereas, other anions such as nitrate tend to act as corrosion inhibitors. Thus, there is a very complex synergism of corrosion effects in the test media.

Table 2. Composition of Standard Test Media Based Upon J-13 Well Water

Ion	SDW (mg/L^{-1})	SCW (mg/L^{-1})	SAW (mg/L^{-1})	SSW (mg/L^{-1})
K^{+1}	3.400E+01	3.400E+03	3.400E+03	1.416E+05
Na^{+1}	4.090E+02	4.090E+04	4.090E+04	4.870E+04
Mg^{+2}	1.000E+00	1.000E+00	1.000E+03	0.000E+00
Ca^{+2}	5.000E-01	1.000E+00	1.000E+03	0.000E+00
F^{-1}	1.400E+01	1.400E+03	0.000E+00	0.000E+00
Cl^{-1}	6.700E+01	6.700E+03	6.700E+03	1.284E+05
NO_3^{-1}	6.400E+01	6.400E+03	6.400E+03	1.310E+06
SO_4^{-2}	1.670E+02	1.670E+04	1.670E+04	0.000E+00
HCO_3^{-1}	9.470E+02	7.000E+04	0.000E+00	0.000E+00
Si	27 (60°C), 49 (90°C)	27 (60°C), 49 (90°C)	27 (60°C), 49 (90°C)	0.000E+00
pH	8.100E+00	8.100E+00	2.700E+00	7.000E+00

NOTE: CRWMS M&O (2000a)

CP measurements have been based on ASTM G 5-87, 1989. The reader should also note the relevance of other procedures such as ASTM G 3-89, 1999 and G 61-86, 1998. Any necessary deviations are noted in the corresponding SN. For example, the procedure calls for sulfuric acid; whereas, simulated Yucca Mountain waters are used here. Furthermore, unlike the procedure, the electrolytes used here were fully aerated. Representative CP curves are shown in Figures 3 and 4 of this report and are categorized as type 2 or 3. All potentials are measured relative to the standard Ag/AgCl reference electrode at ambient temperature (approximately 20°C).

A generic type 1 curve exhibits complete passivity (no passive film breakdown) between the corrosion potential (E_{corr}) and the point defined as threshold potential 1 ($E_{critical}$). This interpretation was verified by visual inspection of samples after potential scans and photographic documentation of some of those samples (all samples are held in the archives at LLNL). Threshold potential 1 is in the range where the onset of oxygen evolution is expected and is defined by a large excursion in anodic current. This particular definition of threshold potential 1 is specific to type 1 curves. Type 1 behavior has only been observed with the WPOB (Alloy 22) and is illustrated by Figures 3 and 4 in the AMR entitled *General and Localized Corrosion of the Waste Package Outer Barrier* (CRWMS M&O 2000d, p. 35). The interpretation of type 1 curves as exhibiting no passive film breakdown is consistent with Section 7 of ASTM G61-86, 1998.

A generic type 2 curve exhibits a well-defined oxidation peak at the point defined as threshold potential 1. Threshold potential 2 is in the range where the onset of oxygen evolution is expected and is defined by a large increase in anodic current. These particular definitions of the threshold potentials are specific to type 2. Repassivation potentials 1 and 2 are defined as the points where the hysteresis loop passes through a current levels of 4.27×10^{-6} and 10^{-5} amps, respectively (not shown). Repassivation potential 3 is determined from the first intersection of the hysteresis loop (reverse scan) with the forward scan. Type 2 is observed with both stainless steel 316L and Alloy 22 and in the case of 316L in SCW at 90°C is illustrated by Figure 3. Scully et al. (1999) define the threshold potential for crevice corrosion of Alloy 22 as the point during the scan of electrochemical potential in the forward direction where the current density increases to a level of 10^{-6} to 10^{-5} A cm^{-2}. Gruss et al. (1998) define the repassivation potential as the point where the current density drops to 10^{-6} to 10^{-7} A cm^{-2}, which is comparable to the definition of repassivation potential 3.

A generic type 3 curve exhibits a complete breakdown of the passive film and active pitting at potentials that are relatively close to the corrosion potential. In this case, threshold potential 1 corresponds to the critical pitting potential. Of the other WP materials tested, type 3 behavior has only been observed with 316L. Figure 4 shows such a CP measurement of stainless steel 316L in SSW at 100°C. This is a saturated sodium-potassium-chloride-nitrate electrolyte, formulated to represent the type of concentrated electrolyte that might evolve on a hot WP surface. This formulation has boiling point of approximately 120°C at ambient pressure.

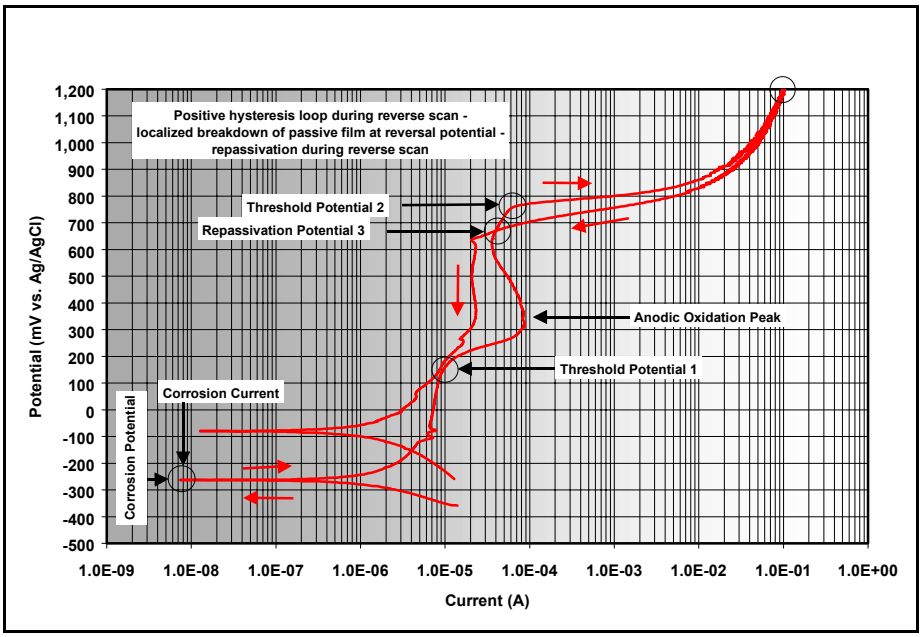

DTN: LL990610105924.074

Figure 3. Type 2 – 316L in SCW at 90°Centigrade (PEA002)

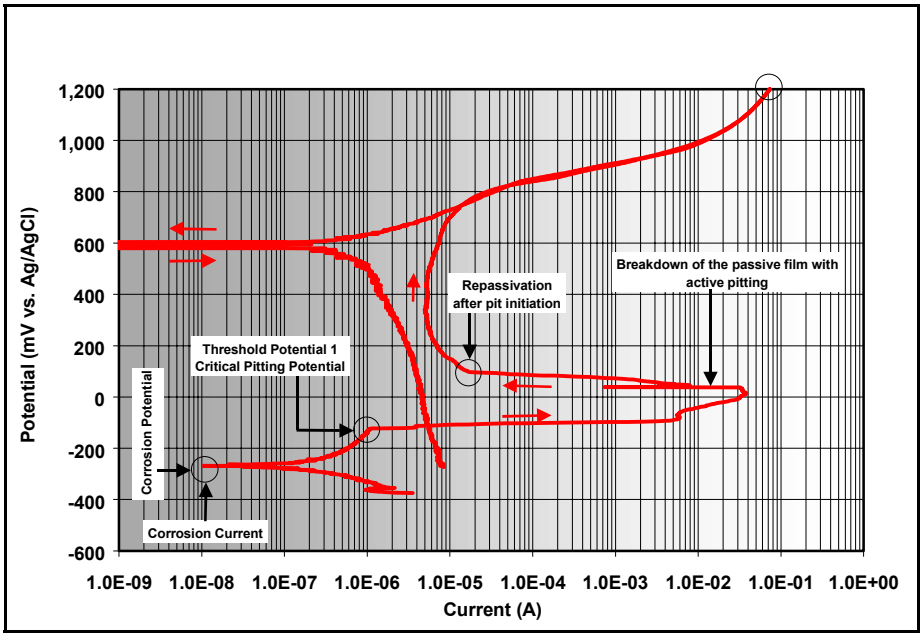

DTN: LL990610105924.074

Figure 4. Type 3 – 316L in SSW at 100°Centigrade (PEA016)

6.4.3 Correlation of Potential versus Temperature Data for Various Test Media

Values of corrosion and threshold potentials are summarized in Table 3 and have been correlated as a function of temperature for the conditions of interest. These correlated data are shown in Figures 5 through 7. In general, it has been found that these potential verses temperature data can be represented by the following simple regression equation:

$$y = b_0 + b_1 x + b_2 x^2 \qquad \text{(Eq. 16)}$$

where y is either the corrosion or threshold potential (mV vs. Ag/AgCl), and x is the temperature (°C). All correlations are summarized in Table 4 with the correlation for E_{corr} and the most conservative correlation for the threshold potential, $E_{critical}$, labeled. In the case of type 2 CP curves, the selected threshold potential is determined by the position of the observed anodic oxidation peak and may not result in any actual loss of passivity. In the case of type 3 CP curves, which are represented by Figure 7, the transparent square represents the range of potential and temperature where pitting attack are believed to be possible. In this case, the various threshold potentials are scattered. The lower boundary of the square appears to be very close to the line representing the corrosion potential. Note that these very low threshold potentials are entirely consistent with the published temperature-dependent pitting potentials given by Sedriks for 316L stainless steel as shown in Figure 8 (Sedriks 1996). These data are represented by the generic expression given in the above equation where b_0 = 547.76, b_1 = -6.617 and b_2 = 0 (Equation 16). Reference to data from Sedriks' book on corrosion of stainless steels is justifiable because this book is used as a reference book in academic institutions (e.g., the University of Nevada, Las Vegas). As this correlation is extrapolated to 100°C, the pitting potential approaches the lower boundary of the transparent box used to bound the threshold potentials in Figure 7.

If YMP designers decide to claim the 316L as a corrosion-resistant inner barrier, the specifications for the WP material include allowable values for E_{corr} and $E_{critical}$. Acceptance of the material requires that: (1) the measured value of E_{corr} in a particular environment cannot exceed the value calculated with the corresponding correlation in Table 4 by more than 24 mV and (2) the measured value of $E_{critical}$ in a particular environment cannot be less than the value calculated with the corresponding correlation in Table 5 by more than 24 mV. These values are determined by splitting the difference between E_{corr} and $E_{critical}$ and are, therefore, different than those given for Alloy 22 (Farmer et al. 1999).

The correlations given in Table 4 were used to calculate the values of E_{corr} and $E_{critical}$ shown in Table 5 for SCW and SAW. The correlation for $E_{critical}$ with temperature in SSW is assumed to be represented by the box shown in Figure 7. According to Bard and Faulkner (1980, back cover) potentials on the Saturated Calomel Electrode (SCE) scale are converted to the Ag/AgCl scale by adding approximately 45 mV to the measured value. According to Jones (1996, p. 66), only 19 mV needs to be added for this conversion.

There are precedents for using electrochemical measurements as the basis of water chemistry and materials specifications in the nuclear industry. For example, measurements of corrosion potential are indicative of dissolved oxygen and can be used to assure adequate deaeration in

various regions of the steam cycle. The role of electrochemical potential on SCC has been well documented by Andresen (1988).

Better correlations of E_{corr} and $E_{critical}$ with material history, water chemistry, and temperature may ultimately allow precise prediction of the crevice corrosion temperature. Improved correlations would provide rigorous statistical estimates of uncertainty and variability in E_{corr} and $E_{critical}$. The precise determination of uncertainty and variability in E_{corr} and $E_{critical}$ would enable designers to determine the impact of accepting 100% of the supplied WP material on repository performance. In the mean time, crevice corrosion can be forced to occur in the model by equating E_{corr} and $E_{critical}$ over temperature ranges of uncertainty. This assumption would provide a conservative estimate of the crevice corrosion temperature. Alternatively, the published data summarized in Figures 9 and 10 can be used to estimate critical temperatures. Improved LC models with accurate temperature dependence will allow a precise sensitivity study, assessing the impact of various WP design changes on the radiological dose at the site boundary.

Table 3. Summary of Cyclic Polarization Data for Stainless Steel 316L in Repository-Relevant Conditions

Sample ID	Electrolyte	Temp.	Corrosion Potential	Threshold Potential 1	Threshold Potential 2	Repassivation Potential 1	Repassivation Potential 2	Repassivation Potential 3
		C	mV	MV	mV	mV	mV	mV
PEA026	SDW	90	UI	573	800	668	708	694
PEA012	SCW	30	-181	422	880	899	917	905
PEA001	SCW	60	-185	283	769	374	750	781
PEA002	SCW	90	-263	135	757	84	80	662
PEA006	SCW	60	-243	298	887	759	800	800
PEA003	SCW	90	-294	179	768	658	681	697
PEA010	SCW	30	-76	422	905	882	907	902
PEA009	SCW	60	-260	263	848	724	752	766
PEA018	SCW	90	-239	194	759	649	666	688
PEA005	SAW	30	-175	454	UI	UI	UI	UI
PEA011	SAW	60	-267	694	1040	964	1020	1030
PEA019	SAW	90	UI	UI	UI	UI	UI	UI
PEA007	SAW	30	UI	UI	UI	UI	UI	UI
PEA013	SAW	60	-363	724	1140	952	1010	1100
PEA008	SAW	30	-227	760	1150	993	1090	1140
PEA014	SAW	60	-286	709	1020	948	1010	1030
PEA015	SAW	60	-294	669	1020	903	975	1020
PEA025	SAW	90	-353	81	none	-216	-225	304
PEA016	SSW	100	-269	-123	none	AP transition	AP transition	AP transition
PEA017	SSW	120	-175	266	998	731	797	942
PEA020	SSW	100	-295	-83	none	AP transition	AP transition	AP transition
PEA021	SSW	120	-208	-80	none	AP transition	AP transition	AP transition
PEA022	SSW	100	-259	-56	none	AP transition	AP transition	AP transition
PEA023	SSW	100	-233	749	943	769	810	777

DTN: LL000201505924.122

Note: UI means that the data was uninterpretable and AP means that the CP curve had and active-passive transition. All potentials were measured with a Ag/AgCl reference electrode. One should subtract 197 mV from measured values to convert to the Normal Hydrogen Electrode (NHE) potential scale.

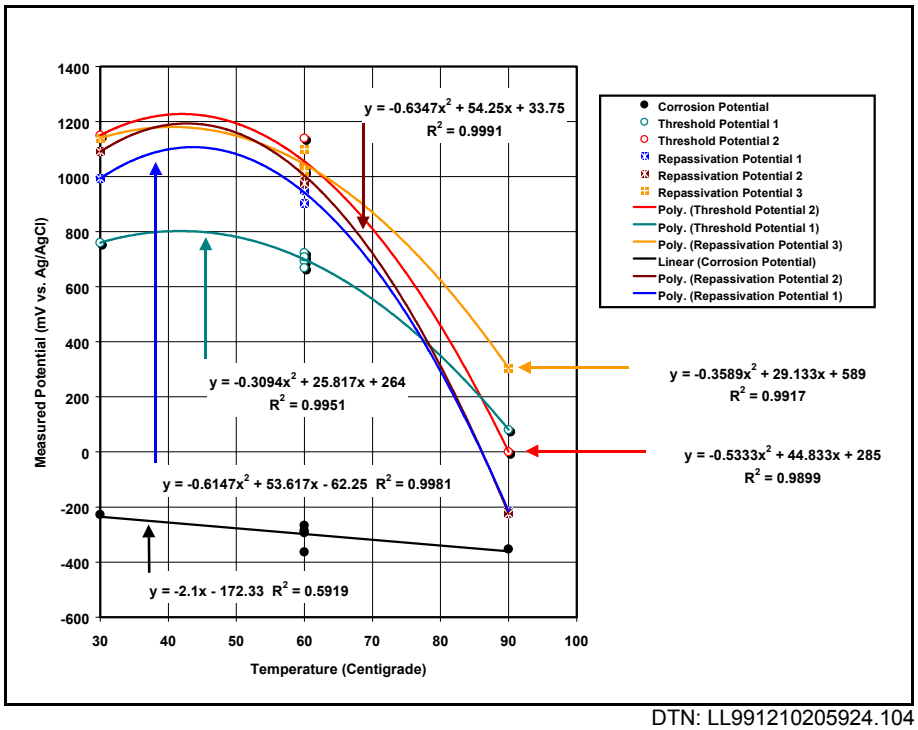

DTN: LL991210205924.104

Figure 5. Potentials versus Temperature: Stainless Steel 316L in SAW

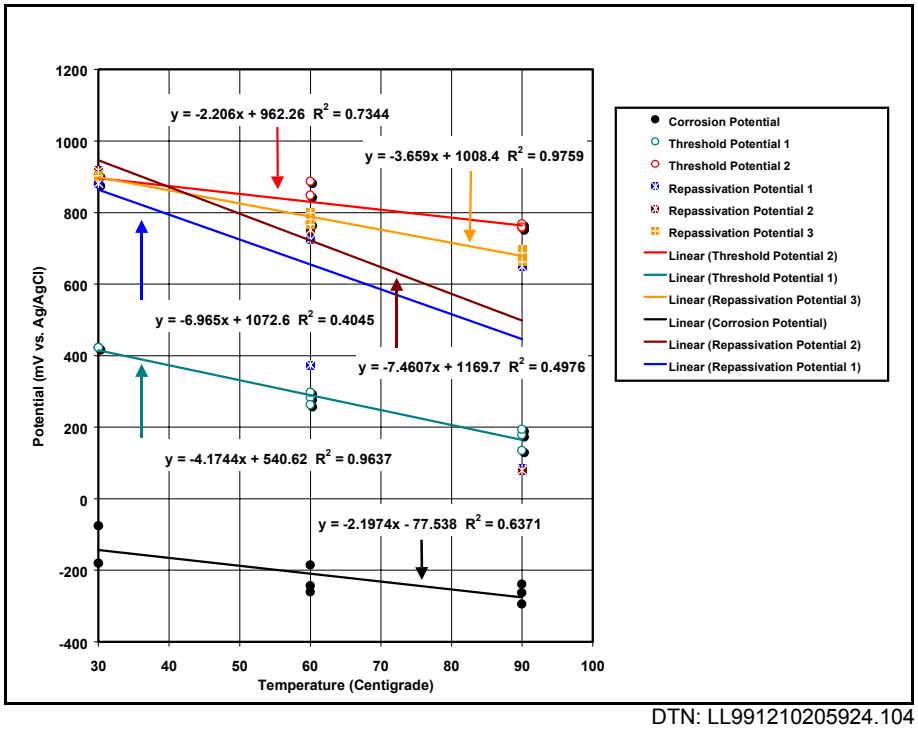

DTN: LL991210205924.104

Figure 6. Potentials versus Temperature: Stainless Steel 316L in SCW

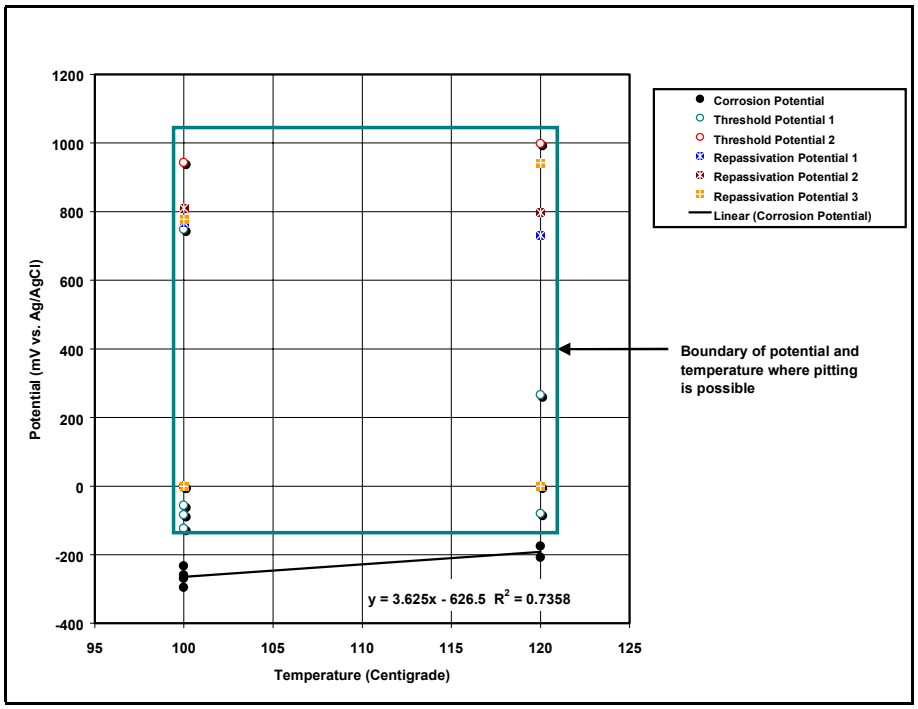

DTN: LL991210205924.104

Figure 7. Potentials versus Temperature: Stainless Steel 316L in SSW

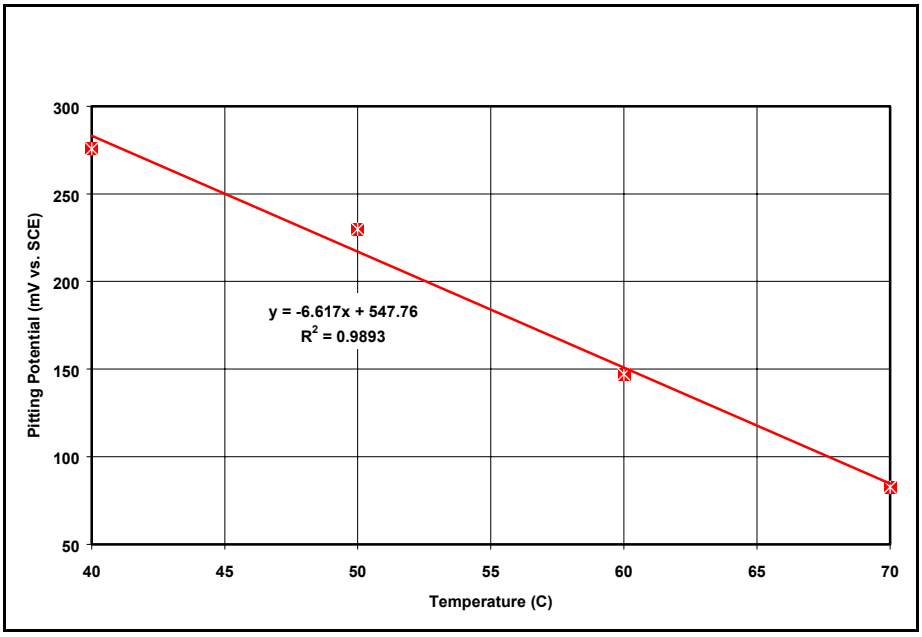

NOTE: Sedriks (1996, Fig. 4.36, p. 145)

Figure 8. Effect of Temperature on the Pitting Potential of Stainless Steel 316L Base Metal in 3.5 Weight Percent NaCl

Table 4. Summary of Correlated Corrosion and Threshold Potential Data

Fig.	Medium	Curve	Potential	Parameter	b_0	b_1	b_2	R^2
5	SAW	Type 2	Corrosion	E_{corr}	-172.33	-2.1		0.5919
5	SAW	Type 2	Threshold 1		264	25.817	-0.3094	0.9951
5	SAW	Type 2	Threshold 2		285	44.833	-0.5333	0.9899
5	SAW	Type 2	Repassivation 1		-62.25	53.617	-0.6147	0.9981
5	SAW	Type 2	Repassivation 2		33.75	54.25	-0.6347	0.9991
5	SAW	Type 2	Repassivation 3	$E_{critical}$	589	29.133	-0.3589	0.9917
6	SCW	Type 2	Corrosion	E_{corr}	-77.538	-2.1974		0.6371
6	SCW	Type 2	Threshold 1	$E_{critical}$	540.62	-4,1744		0.9637
6	SCW	Type 2	Threshold 2		962.26	-2.206		0.7344
6	SCW	Type 2	Repassivation 1		1072.6	-6.965		0.4045
6	SCW	Type 2	Repassivation 2		1169.7	-7.4607		0.4976
6	SCW	Type 2	Repassivation 3		1008.4	-3.659		0.9759
7	SSW	Type 3	Corrosion	E_{corr}	-626.5	3.625		0.7358
7	SSW	Type 3	Threshold 1	$E_{critical} - 45$	547.75	-6.617		0.9893

DTN: LL991210205924.104

Table 5. Values of E_{corr} and $E_{critical}$ Based on Correlated Cyclic Polarization Data

	SCW	SCW	SCW	SAW	SAW	SAW	SSW	SSW	SSW
T	E_{corr}	$E_{critical}$	Diff.	E_{corr}	$E_{critical}$	Diff.	E_{corr}	$E_{critical}$	Diff.
°C	mV	mV	MV	mV	mV	mV	mV	mV	MV
20	-121	457	579	-214	1028	1242	-554	415	969
30	-143	415	559	-235	1140	1375	-518	349	867
40	-165	374	539	-256	1180	1436	-482	283	765
50	-187	332	519	-277	1148	1426	-445	217	662
60	-209	290	500	-298	1045	1343	-409	151	560
70	-231	248	480	-319	870	1189	-373	85	457
80	-253	207	460	-340	623	963	-337	18	355
90	-275	165	440	-361	304	665	-300	-48	252
100	-297	123	420	-382	-87	296	-264	-114	150
110							-228	-180	48
120							-192	-246	-55
130							-155	-312	-157
140							-119	-379	-260
150							-83	-445	-362

DTN: LL991210305924.105

6.4.4 Correction of Measured Potential for Junction Potential

All potentials are measured relative to the standard Ag/AgCl reference electrode at ambient temperature (approximately 20°C). The filling solution of the reference electrode was 4 M KCl, saturated with AgCl. The low temperature of the reference electrode was maintained at ambient temperature during experiments with heated electrochemical cells by using a water-cooled Luggin probe filled with 4M KCl in all tests except those with SSW above 100°C. In these experiments, which were above the boiling point of 4M KCl, SSW was used to fill the Luggin probe. Filling the Luggin probe with KCl solution is a slight deviation from ASTM Procedure G 5-87, 1989 that could lead to introduction of additional chloride anion into the test medium. However, given the relatively high concentration of chloride already in the test medium, this is not believed to be a significant problem.

It is important to understand the error in the potential measurements due to the concentration-dependent junction potential. A correction has been performed based upon the Henderson Equation (Bard & Faulkner 1980). Ionic properties used in the calculation were taken from the same reference (Bard & Faulkner 1980). Calculated values of E_j for the isothermal junction are summarized in Table 6.

Table 6. Summary of Junction Potential Corrections for CP (volts)

T (°C)	SDW	SCW	SAW	SSW
30	2.716E-03	1.188E-03	6.019E-03	-7.649E-03
60	2.984E-03	1.306E-03	6.615E-03	-8.406E-03
90	3.253E-03	1.423E-03	7.210E-03	-9.164E-03

DTN: LL991208405924.098

These corrections are not very large, with the largest being about 9 mV for SCW, and have been justifiably ignored in the present data analysis. The effects of temperature across the Luggin probe are assumed to be negligible.

6.4.5 Prediction of Critical Temperatures for Pitting and Crevice Corrosion

As previously discussed, a threshold temperature (critical temperature) can be used as an alternative to a threshold potential for the initiation of LC. In an ideal case, the critical temperatures for pitting and crevice corrosion can be estimated from the intersection of the lines representing the corrosion and threshold potentials as functions of temperature. This intersection occurs at elevated temperature. The critical temperature for pitting of stainless steel 316L is illustrated by Figures 9 and 10. To force crevice corrosion to occur in the model, E_{corr} and $E_{critical}$ can simply be equated above the critical temperature.

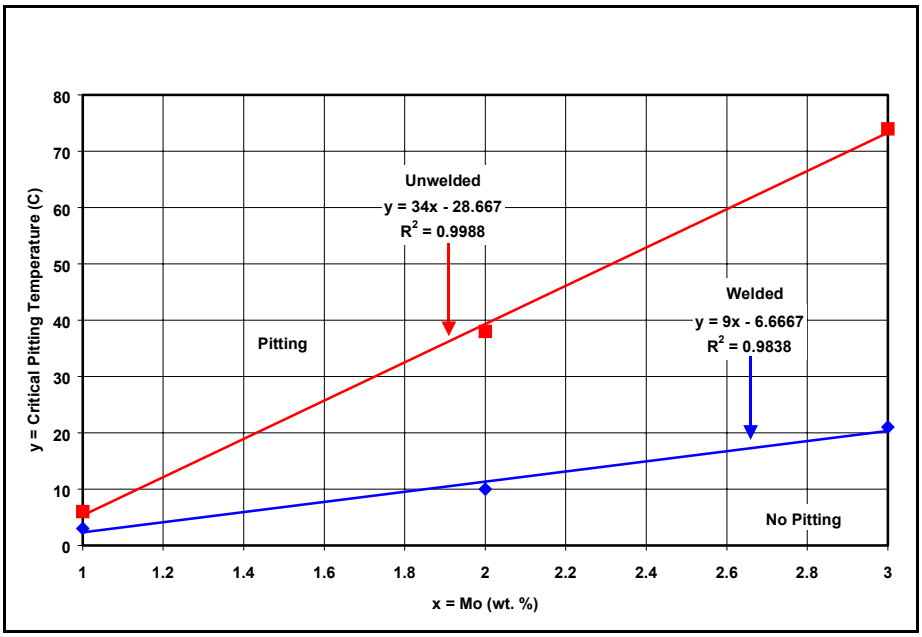

NOTE: Sedriks (p. 112, Fig. 4.9, Ref. 50)

Figure 9. Effect of Molybdenum on the Critical Pitting Temperature of Stainless Steels in Ferric Chloride Solution

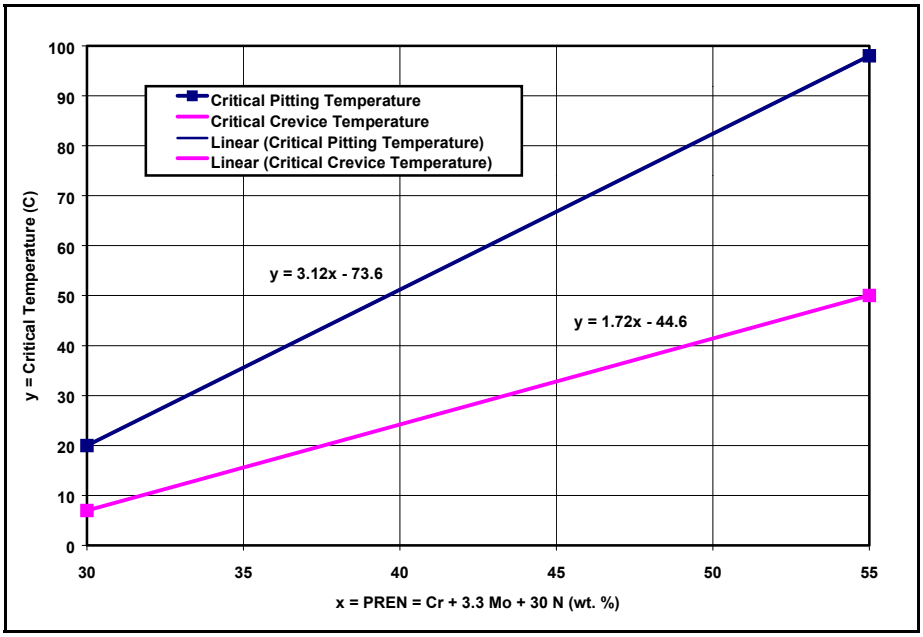

NOTE: Sedriks (p. 113, Fig. 4.10, Ref. 58)

Figure 10. Effect of Pit Resistance Equivalence Number (PREN) on the Critical Pitting and Crevice Corrosion Temperature of Stainless Steels in Ferric Chloride Solution

6.5 RATES OF GENERAL AND LOCALIZED CORROSION

LC rates will be assumed if the open circuit corrosion potential (E_{corr}) exceeds the conservative threshold potential ($E_{critical}$). GC rates will be assumed if the threshold potential is not exceeded. The distribution of GC and LC rates will be estimated from the published data for 304 and 316 stainless steel that is summarized statistically in Tables 7, 8, and 9 as well as in Figures 11 and 12. GC rates were taken from one source (Gdowski and Bullen 1988, pp. 16, 20-21) while LC rates were taken from another (Farmer et al. 1988, pp. 28-29). As an alternative, the distribution of LC rates can also be estimated from the published data that is summarized in Tables 10a, 10b and 10c as well as in Figures 13 and 14 (Sedriks 1996). Curves are shown for GC in atmospheric environments, GC in aqueous-phase environments, and LC in aqueous-phase environments. The corresponding distributions can be represented by the following general correlation:

$$y = b_0 + b_1 x \qquad \text{(Eq. 17)}$$

where y is the cumulative probability or percentile, and x is the logarithm of the corrosion rate, which is expressed in microns per year. Parameters are given in Table 11. These cumulative distribution functions (CDFs) are truncated for any nonsensical calculated values above 100%. These distributions do not reflect any environmental dependence since such a correlation could not be established based upon the published data. It is assumed that these distributions are primarily due to variability. In lieu of rigorous estimates of uncertainty, the uncertainty is assumed to be comparable to the variability. In the future, more work is needed to introduce environmental dependence and to separate variability and uncertainty.

Published rates of GC and LC are summarized in Tables 6 through 9 as well as in Figures 11 through 14. From comparing the data for 304 and 316 stainless steels, the advantages of molybdenum additions are evident. The corrosion rates of 304 are higher than comparable rates of 316. Type 316 stainless steel contains more molybdenum than Type 304 stainless steel. From Figure 12, the LC rates of 316 appear to lie between 10^3 and 10^4 μm y^{-1}. The GC rates for APC of 316 appear to lie between 10^{-1} and 10^2 μm y^{-1}. The GC rates for HAC (atmospheric corrosion) of 316 appear to lie between 10^{-3} and 10^{-1} μm y^{-1}. It is assumed that the published rates for 316 are representative of those for 316NG. The regression line shown in Figure 12 is assumed to represent both uncertainty and variability.

Table 7. General Corrosion Rates for Atmospheric and Aqueous Phase Exposure of Stainless Steel 304

Alloy	Mode	Environment	Weight Loss	Corrosion Rate	Exposure	Source	Place
			$mg/dm^2/day$	microns/year	years	UCID-21362 Vol. 2	
304	General Atmospheric	Marine	0.062	0.283	11.880	Table 2	Bayonne, NJ
304	General Atmospheric	Marine	0.000	0.000	11.880	Table 2	Bayonne, NJ
304	General Atmospheric	Urban	0.043	0.195	5.000	Table 2	Sheffield, England
304	General Atmospheric	Urban	0.017	0.078	5.000	Table 2	Sheffield, England
304	General Atmospheric	Urban	0.012	0.055	5.000	Table 2	Sheffield, England
		Average	0.027	0.122			
304	General Aqueous	Sea Water	5.910	26.960	0.340	Table 3	Depth of 5640 ft
304	General Aqueous	Sea Water	8.510	38.830	2.060	Table 3	Depth of 5640 ft
304	General Aqueous	Sea Water	5.310	24.230	2.920	Table 3	Depth of 5300 ft
304	General Aqueous	Sea Water	3.150	14.370	1.060	Table 3	Ocean Surface
304	General Aqueous	Sea Water		56.760	1.340	Table 3	Quiescent Sea Water
304	General Aqueous	Sea Water		14.280	1.780	Table 3	Quiescent Sea Water
304	General Aqueous	River Water		65.770	0.300	Table 3	Colorado River, Cl ~ 100 mg/L
304	General Aqueous	River Water		40.560	0.250	Table 3	Colorado River, Cl ~ 200 mg/L
304	General Aqueous	River Water		533.330	0.300	Table 3	Colorado River, Cl ~ 300 mg/L
304	General Aqueous	River Water		91.250	0.330	Table 3	Colorado River, Cl ~ 600 mg/L
304	General Aqueous	River Water		81.110	0.500	Table 3	Colorado River, Cl ~ 1000 mg/L
		Average	5.720	89.768			
304	Steam	Steam	0.760	3.470	1.130	Table 3	Superheated at 566 C
304	Steam	Steam	2.123	9.690	1.130	Table 3	Superheated at 621 C
		Average	1.442	6.580			

DTN: LL991210405924.106

NOTE: Gdowski and Bullen (1988)

Table 8. General Corrosion Rates for Atmospheric Exposure of Stainless Steel 316

Alloy	Mode	Environment	Weight Loss	Corrosion Rate	Exposure	Source	Place
			$mg/dm^2/day$	microns/year	years	UCID-21362 Vol. 2	
316	General Atmospheric	Marine	0.000	0.000	11.880	Table 2	Bayonne, NJ
316	General Atmospheric	Marine	0.000	0.000	11.880	Table 2	Bayonne, NJ
316	General Atmospheric	Marine	0.000	0.000	1.000	Table 2	Panama Canal
316	General Atmospheric	Marine	0.000	0.000	8.000	Table 2	Panama Canal
316	General Atmospheric	Marine	0.000	0.000	16.000	Table 2	Panama Canal
316	General Atmospheric	Marine	0.007	0.033	5.000	Table 2	Kure Beach, NC
316	General Atmospheric	Marine	0.000	0.000	5.000	Table 2	Kure Beach, NC
316	General Atmospheric	Rural-marine	0.000	0.000	2.000	Table 2	Halifax, Canada
316	General Atmospheric	Rural-marine	0.000	0.000	2.000	Table 2	Esquimault, Canada
316	General Atmospheric	Urban	0.002	0.009	5.000	Table 2	Sheffield, England
316	General Atmospheric	Urban	0.003	0.014	5.000	Table 2	Sheffield, England
316	General Atmospheric	Urban	0.003	0.014	5.000	Table 2	Sheffield, England
316	General Atmospheric	Urban	0.003	0.014	5.000	Table 2	Sheffield, England
316	General Atmospheric	Industrial	0.002	0.008	4.920	Table 2	Bridgeport, CT
316	General Atmospheric	Industrial	0.000	0.000	2.000	Table 2	Montreal, Canada
316	General Atmospheric	Industrial	0.007	0.030	2.000	Table 2	Halifax, Canada
316	General Atmospheric	Rural	0.000	0.000	1.000	Table 2	Panama Canal
316	General Atmospheric	Rural	0.000	0.000	8.000	Table 2	Panama Canal
316	General Atmospheric	Rural	0.000	0.000	16.000	Table 2	Panama Canal
316	General Atmospheric	Rural	0.000	0.000	2.000	Table 2	Saskatoon, Canada
316	General Atmospheric	Semirural	0.000	0.000	2.000	Table 2	Ottawa, Canada
316	General Atmospheric	Semirural	0.000	0.000	2.000	Table 2	Trail, Canada
		Average	0.001	0.006			

DTN: LL991210405924.106

NOTE: Gdowski and Bullen (1988)

Table 9. General Corrosion Rates for Aqueous Phase Exposure of Stainless Steel 316

Alloy	Mode	Environment	Weight Loss	Corrosion Rate	Exposure	Source	Place
			$mg/dm^2/day$	microns/year	years	UCID-21362 Vol. 2	
316	General Aqueous	Sea Water	3.285	14.990	1.000	Table 3	Panama Canal - Imersion Test
316	General Aqueous	Sea Water	1.403	6.400	8.000	Table 3	Panama Canal - Imersion Test
316	General Aqueous	Sea Water	0.274	1.250	16.000	Table 3	Panama Canal - Imersion Test
316	General Aqueous	Sea Water	0.274	1.250	16.000	Table 3	Panama Canal - Mean Tide
316	General Aqueous	Sea Water	0.137	0.630	8.000	Table 3	Panama Canal - Mean Tide
316	General Aqueous	Sea Water	0.034	0.160	16.000	Table 3	Panama Canal - Mean Tide
316	General Aqueous	Sea Water	0.890	4.060	1.320	Table 3	Flowing Sea Water - Pitting
316	General Aqueous	Sea Water	0.340	1.550	4.500	Table 3	Flowing Sea Water - Pitting
316	General Aqueous	Sea Water	1.340	6.110	1.320	Table 3	Stagnant Sea Water - Pitting
316	General Aqueous	Sea Water		18.920	1.340	Table 3	Quiescent Sea Water
316	General Aqueous	Sea Water		57.140	1.780	Table 3	Quiescent Sea Water
		Average	0.886	10.224			
316	General Aqueous	Lake Water	0.000	0.000	1.000	Table 3	Panamal Canal - Imersion Test
316	General Aqueous	Lake Water	0.000	0.000	8.000	Table 3	Panamal Canal - Imersion Test
316	General Aqueous	Lake Water	0.000	0.000	16.000	Table 3	Panamal Canal - Imersion Test
316	General Aqueous	River Water		0.000	0.300	Table 3	Colorado River, Cl ~ 100 mg/L
316	General Aqueous	River Water		0.000	0.250	Table 3	Colorado River, Cl ~ 200 mg/L
316	General Aqueous	River Water		0.000	0.300	Table 3	Colorado River, Cl ~ 300 mg/L
316	General Aqueous	River Water		0.000	0.330	Table 3	Colorado River, Cl ~ 600 mg/L
316	General Aqueous	River Water		0.000	0.500	Table 3	Colorado River, Cl ~ 1000 mg/L
		Average	0.000	0.000			

DTN: LL991210405924.106

NOTE: Gdowski and Bullen (1988)

Table 10a. Rates of Localized Corrosion for Stainless Steel 304 and 316 in Various Environments

Data Set	LC Mode	Rate	Material & Environment	Penetration Rate (mm/yr)
1	Crevice	1.12 mm/yr	Fe-18Cr-9Ni & 0.5 N NaCl	1.12000
1	Crevice	1.30 mm/yr	Fe-18Cr-9Ni & 0.5 N NaCl	1.30000
2	Crevice	0 mg/cm^2	Alloy C & Sea Water	0.00000
2	Crevice	9.07 mg/cm^2	316 & Sea Water	0.01134
2	Crevice	10.93 $mg.cm^2$	304 & Sea Water	0.01366
3	Crevice	0.002,0.004,0.046 g/m^2/day	Cold Rolled 316 & Sea Water	0.00210
3	Crevice	0.06,0.54,0.54 g/m^2/day	316 & Sea Water	0.02464
4	Crevice	0.28 mm	304 & Sea Water	3.36000
4	Crevice	0.03 mm	316 & Sea Water	0.36000
5	Crevice	64 mg/dm^2/day	Fe-20Cr-2Mo	0.89881
5	Crevice	197 mg/dm^2/day	Fe-20Cr-2Mo	0.20988
6	Crevice	2.20 mm & 38 sites attacked	316 with Carbon Steel (1:0 ratio)	26.40000
6	Crevice	2.73 mm & 18 sites attacked	316 with Carbon Steel (1:0 ratio)	10.92000
6	Crevice	0 mm	316 with Carbon Steel (3:1 ratio)	0.00000
6	Crevice	0 mm	316 with Carbon Steel (10:1 ratio)	0.00000
6	Crevice	0 mm	316 with Carbon Steel (10:1 ratio)	0.00000
6	Crevice	0.02 mm & 5 sites attacked	316 with Carbon Steel (50:1 ratio)	0.24000
7	Pitting	16.13 mg/in2 & 14.1 $pits/in^2$	301 with 0.03% Mo	
7	Pitting	10.6 mg/in2 & 3.5 $pits/in^2$	301 with 0.26% Mo	
7	Pitting	8.3 mg/in2 & 2.4 $pits/in^2$	301 with 0.51% Mo	
7	Pitting	8.3 mg/in2 & 0.8 $pits/in^2$	301 with 0.75% Mo	
7	Pitting	1.7 mg/in2 & 0.49 $pits/in^2$	316 with 0.007% S	
7	Pitting	8.8 mg/in2 & 0.22 $pits/in^2$	316 with 0.017% S	
7	Pitting	5.6 mg/in2 & 0.82 $pits/in^2$	316 with 0.040% S	
7	Pitting	17.3 mg/in2 & 1.64 $pits/in^2$	316 with 0.320% S	
8	Pitting	1.98 mm max. & 0.96 mm avg.	316 - Plate	0.55721
8	Pitting	3.30 mm max. & 1.93 mm avg.	316 - Weld	0.92868
9	Pitting	0.028 mm avg.	304	0.00187
9	Pitting	0.025 mm avg.	316	0.00167

Table 10b. Rates of Localized Corrosion for Stainless Steel 304 and 316 in Various Environments

Data Set	Material	Environment
1	Fe-18Cr-9Ni	0.5 N NaCl for 100 days
1	Fe-18Cr-9Ni	0.5 N NaCl for 100 days
2	Alloy C	Sea Water for 4.25 years
2	Stainless Steel 316	Sea Water for 4.25 years
2	Stainless Steel 304	Sea Water for 4.25 years
3	Stainless Steel 316 - Cold Rolled	Sea Water
3	Stainless Steel 316 - Annealed	Sea Water
4	Stainless Steel 304	Sea Water for 30 days at 15 C
4	Stainless Steel 316	Sea Water for 30 days at 15 C
5	Fe-20Cr-2Mo	10 wt.% FeCl3-6H2O + 0.1 N HCl at 25 C
5	Fe-20Cr-2Mo	10 wt.% FeCl3-6H2O + 0.1 N HCl at 25 C
6	Stainless Steel 316 with Carbon Steel (1:0 ratio)	Sea Water for 30 days at 28 C
6	Stainless Steel 316 with Carbon Steel (1:0 ratio)	Sea Water for 90 days at 22 C
6	Stainless Steel 316 with Carbon Steel (3:1 ratio)	Sea Water for 30 days at 28 C
6	Stainless Steel 316 with Carbon Steel (10:1 ratio)	Sea Water for 30 days at 28 C
6	Stainless Steel 316 with Carbon Steel (10:1 ratio)	Sea Water for 90 days at 22 C
6	Stainless Steel 316 with Carbon Steel (50:1 ratio)	Sea Water for 30 days at 28 C
7	Stainless Steel 301 with 0.03% Mo	108 g FeCl3-6H2O + 4.15 cc HCl in 1 L at 30 C
7	Stainless Steel 301 with 0.26% Mo	108 g FeCl3-6H2O + 4.15 cc HCl in 1 L at 30 C
7	Stainless Steel 301 with 0.51% Mo	108 g FeCl3-6H2O + 4.15 cc HCl in 1 L at 30 C
7	Stainless Steel 301 with 0.75% Mo	108 g FeCl3-6H2O + 4.15 cc HCl in 1 L at 30 C
7	Stainless Steel 316 with 0.007% S	108 g FeCl3-6H2O + 4.15 cc HCl in 1 L at 30 C
7	Stainless Steel 316 with 0.017% S	108 g FeCl3-6H2O + 4.15 cc HCl in 1 L at 30 C
7	Stainless Steel 316 with 0.040% S	108 g FeCl3-6H2O + 4.15 cc HCl in 1 L at 30 C
7	Stainless Steel 316 with 0.320% S	108 g FeCl3-6H2O + 4.15 cc HCl in 1 L at 30 C
8	Stainless Steel 316 - Plate	Sea Water for 1257 days
8	Stainless Steel 316 - Weld	Sea Water for 1257 days
9	Stainless Steel 304	250 m from ocean - Kure Beach, NC - 15 years
9	Stainless Steel 316	250 m from ocean - Kure Beach, NC - 15 years

Table 10c. Rates of Localized Corrosion for Stainless Steel 304 and 316 in Various Environments

Data Set	Reference	Comments
1	Sedriks p. 189 Fig. 5.4 Ref.	0.23 cm2 attacked; 15 cm2 in crevice; medicinal rubber
1	Sedriks p. 189 Fig. 5.4 Ref.	0.20 cm2 attacked; 15 cm2 in crevice; medicinal rubber
2	Sedriks p. 190 Fig. 5.10 Ref. 32	Ep-Ex = 0 mV
2	Sedriks p. 190 Fig. 5.10 Ref. 32	Ep-Ex = 75.76 mV
2	Sedriks p. 190 Fig. 5.10 Ref. 32	Ep-Ex = 103.54 mV
3	Sedriks p. 191 Table 5.5 Ref. 32 & 33	Ep-Ex = 60,60,60 mV
3	Sedriks p. 191 Table 5.5 Ref. 32 & 33	Ep-Ex = 350,360,240 mV
4	Sedriks p. 203 Table 5.6 Ref. 62	Probability of Crevice Attack = 13% (120 Crevices)
4	Sedriks p. 203 Table 5.6 Ref. 62	Probability of Crevice Attack = 2% (120 Crevices)
5	Sedriks p. 203 Table 5.7 Ref. 63	Single day of exposure
5	Sedriks p. 203 Table 5.7 Ref. 63	Single day of exposure
6	Sedriks p. 218 Table 5.13 Ref. 103	Flow rate of 0.5 m/s
6	Sedriks p. 218 Table 5.13 Ref. 103	Flow rate of 0.5 m/s
6	Sedriks p. 218 Table 5.13 Ref. 103	Flow rate of 0.5 m/s
6	Sedriks p. 218 Table 5.13 Ref. 103	Flow rate of 0.5 m/s
6	Sedriks p. 218 Table 5.13 Ref. 103	Flow rate of 0.5 m/s
6	Sedriks p. 218 Table 5.13 Ref. 103	Flow rate of 0.5 m/s
7	Sedriks p. 109 Table 4.2 Ref. 43	Period of exposure unknown
7	Sedriks p. 109 Table 4.2 Ref. 43	Period of exposure unknown
7	Sedriks p. 109 Table 4.2 Ref. 43	Period of exposure unknown
7	Sedriks p. 109 Table 4.2 Ref. 43	Period of exposure unknown
7	Sedriks p. 109 Table 4.2 Ref. 43	Period of exposure unknown
7	Sedriks p. 109 Table 4.2 Ref. 43	Period of exposure unknown
7	Sedriks p. 109 Table 4.2 Ref. 43	Period of exposure unknown
7	Sedriks p. 109 Table 4.2 Ref. 43	Period of exposure unknown
8	Sedriks p. 158 p. 158 Table 4.14 Ref. 215	Stagnant flow & 87 pits; area unknown
8	Sedriks p. 158 p. 158 Table 4.14 Ref. 215	Stagnant flow & 47 pits; area unknown
9	ASM Specialty Handbook p. 150 Table 13	Spotted with slight rust stain on 15% of surface
9	ASM Specialty Handbook p. 150 Table 13	Extremely slight rust stain on 15% of surface

NOTE: Sedriks (1996); ASM (1994)

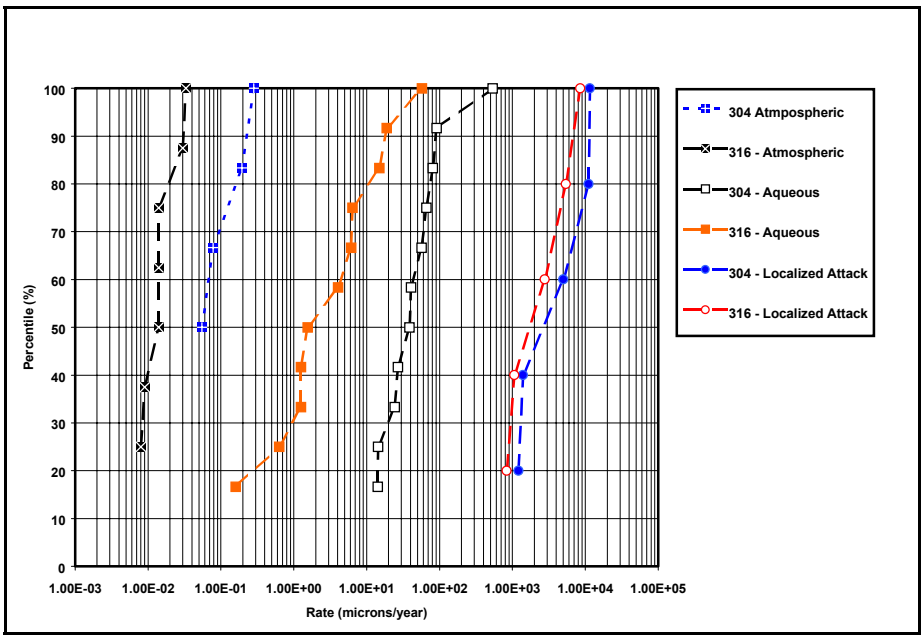

DTN: LL991210405924.106

NOTE: Data taken from Gdowski and Bullen (1988, p. 16, 20-21); Farmer et al. (1988, pp. 28-29)

Figure 11. Range of Observed Penetration Rates for Stainless Steels 304 and 316

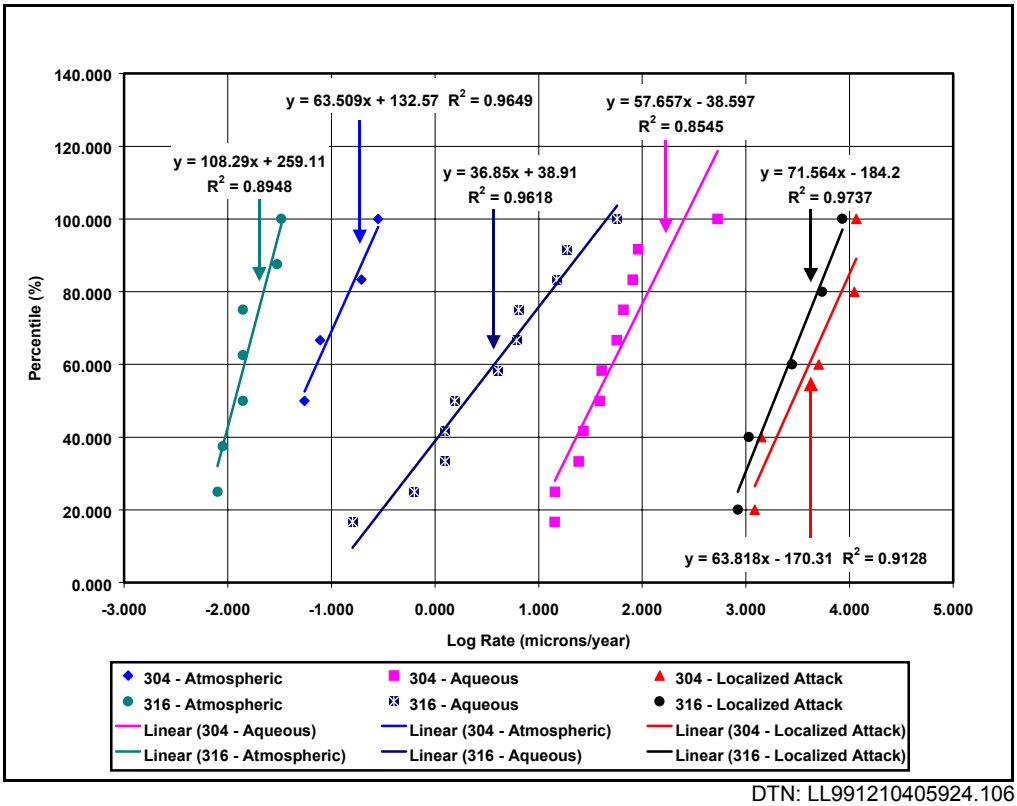

DTN: LL991210405924.106

NOTE: Data taken from Gdowski and Bullen (1988, pp. 16, 20-21); Farmer et al. (1988, pp. 28-29)

Figure 12. Range of Observed Logarithms of Penetration Rates for Stainless Steels 304 and 316

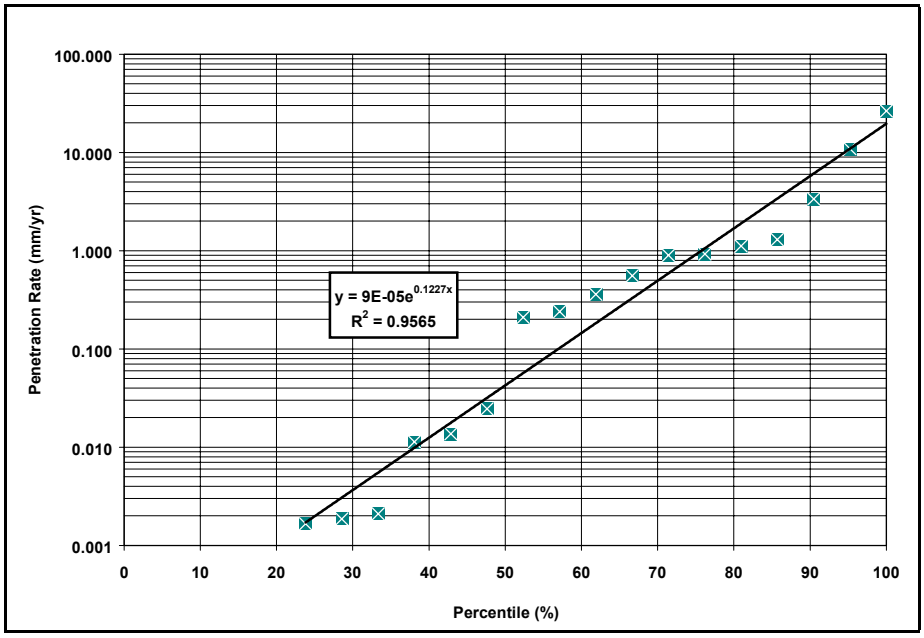

DTN: LL991210405924.106

NOTE: Data taken from Sedriks (1996, Table 4.2, p. 109; Table 5.4, p. 189; Figure 5.10, p. 190; Table 5.5, p. 191; Table 5.6 & 5.7, p. 203; Table 5.13, p. 218; Table 4.14, p. 158) (ASM Handbook, Table 13, p. 150)

Figure 13. Range of Localized Penetration Rates for Stainless Steels 304 and 316

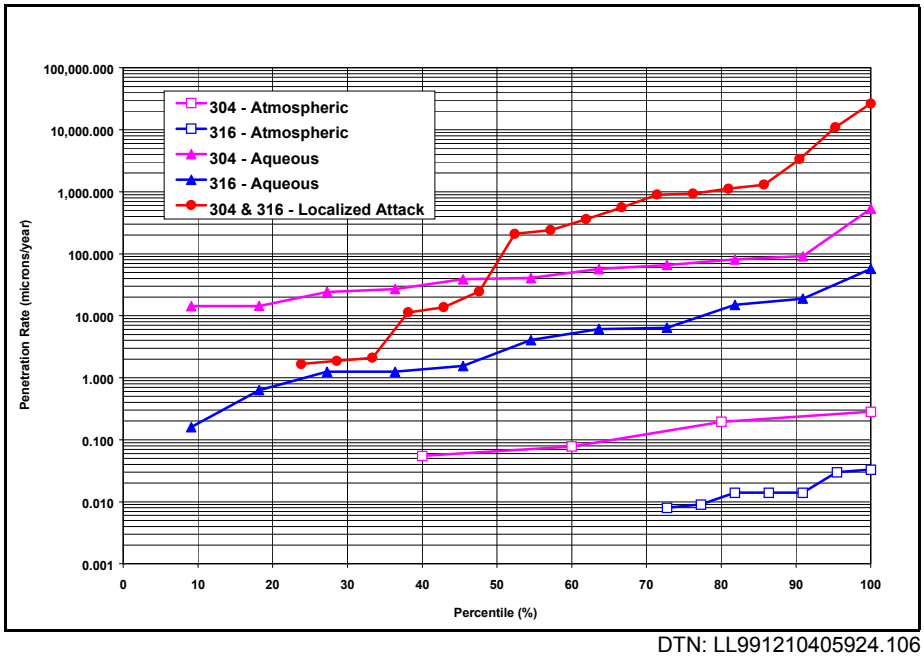

DTN: LL991210405924.106

NOTE: Data taken from Sedriks (1996, Table 4.2, p. 109; Table 5.4, p. 189; Figure 5.10, p. 190; Table 5.5, p. 191; Table 5.6 & 5.7, p. 203; Table 5.13, p. 218; Table 4.14, p. 158) (ASM Handbook, Table 13, p. 150) (Gdowski and Bullen 1988, pp. 16, 20-21)

Figure 14. Comparison of Observed Penetration Rates for Stainless Steels 304 and 316 from Sedriks and Degradation Mode Surveys

Table 11. Summary of Correlated Corrosion and Threshold Potential Data

Material	Environment	Mode	b_0	b_1	R^2
304	Atmospheric	General	132.57	63.509	0.9649
304	Aqueous Phase	General	-38.597	57.657	0.8545
304	Aqueous Phase	Localized	-170.31	63.818	0.9128
316	Atmospheric	General	259.11	108.29	0.8948
316	Aqueous Phase	General	38.91	36.85	0.9618
316	Aqueous Phase	Localized	-184.2	71,564	0.9737

DTN: LL991210605924.107

6.6 EFFECT OF GAMMA RADIOLYSIS ON CORROSION POTENTIAL

Anodic shifts in the open circuit corrosion potential of stainless steel have been experimentally observed (Glass et al. 1986; Kim 1987, 1988, 1999a, 1999b). It is now accepted as fact by much of the engineering community that this observation is due to the generation of hydrogen peroxide. Consequently, this data is treated as "accepted data" rather than "corroborative data" in this AMR.

This observation is evident from the pioneering work of Glass et al. (1986). He performed ambient-temperature CP of 316L samples in 0.018 M NaCl solution during exposure to 3.5 Mrad h^{-1} gamma radiation. The corrosion potential (E_{corr}) shifted in the anodic direction by approximately 200 mV with very little increase in the corresponding corrosion current density (corrosion rate). However, the separation between the corrosion potential and the threshold for localized attack decreased correspondingly. This shift in corrosion potential was shown to be due to the formation of hydrogen peroxide. Kim (1987, 1988, 1999a, 1999b) subsequently confirmed this finding. In this case, ambient-temperature CP of 316 stainless steel in acidic (pH~2) 1.5 M NaCl during exposure to 0.15 Mrad h^{-1} gamma radiation showed a 100 mV anodic shift in the corrosion potential with very little effect on the corrosion current. It will be assumed that gamma radiolysis can cause shifts of approximately 200 mV, which may lead to LC of 316NG stainless steel.

6.7 CREVICE CORROSION

6.7.1 Scenarios Leading to Crevice Formation

Crevices can form at points of contact between the WP and other solid objects. These occluded geometries can lead to differential aeration of the crevice solution (electrolyte). Dissolved oxygen can become depleted deep within the crevice, while the concentration near the crevice mouth remains relatively high. Cathodic reduction of dissolved oxygen at the crevice mouth may create a sufficiently high electrochemical potential to drive anodic processes inside the crevice, thereby causing an anodic current to flow along the crevice towards the crevice mouth. Anodic processes inside the crevice are, therefore, expected to occur at a rate that corresponds to the local passive current density. Two primary electrochemical processes can lead to acidification of the solution in a crevice: (1) the preferential transport of anions into the crevice from the mouth, driven by the electric field that accompanies the crevice current and (2) hydrolysis reactions of dissolved metal cations. For example, pH < 2 has been observed in crevices made of steels containing more than 20 wt.% chromium. The effect of chromium

content on the ultimate crevice pH in a number of commercial and binary Fe-Cr alloys is illustrated by Figure 15 (Sedriks 1996, p. 179). The increase in concentration of dissolved metals in such crevices is illustrated by Figure 16 (Sedriks 1996, p. 184).

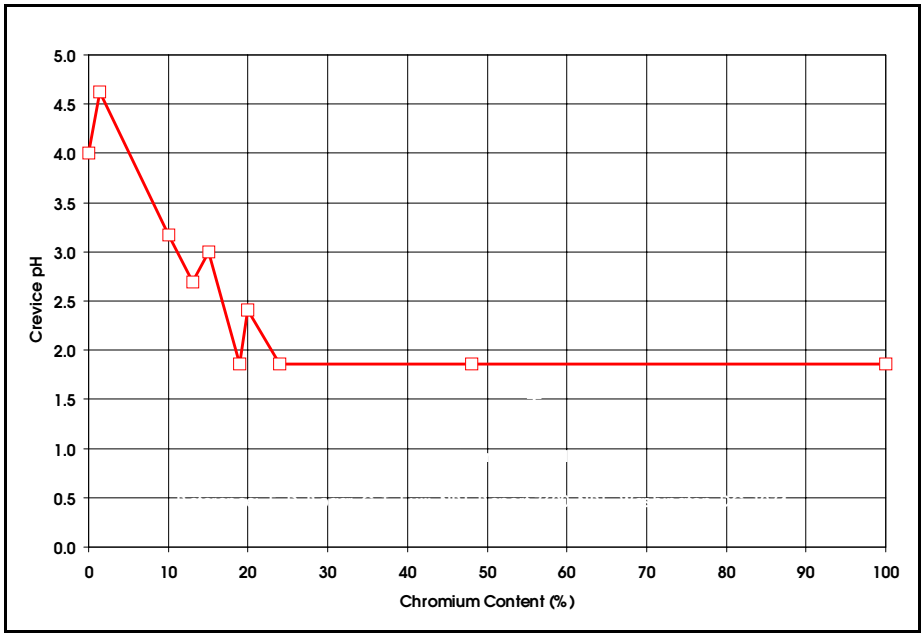

NOTE: Sedriks (1996, Figure 5.3, p. 179, Ref. 6)

Figure 15. Effect of Chromium Content in Ni-Cr Alloys on Ultimate Crevice pH

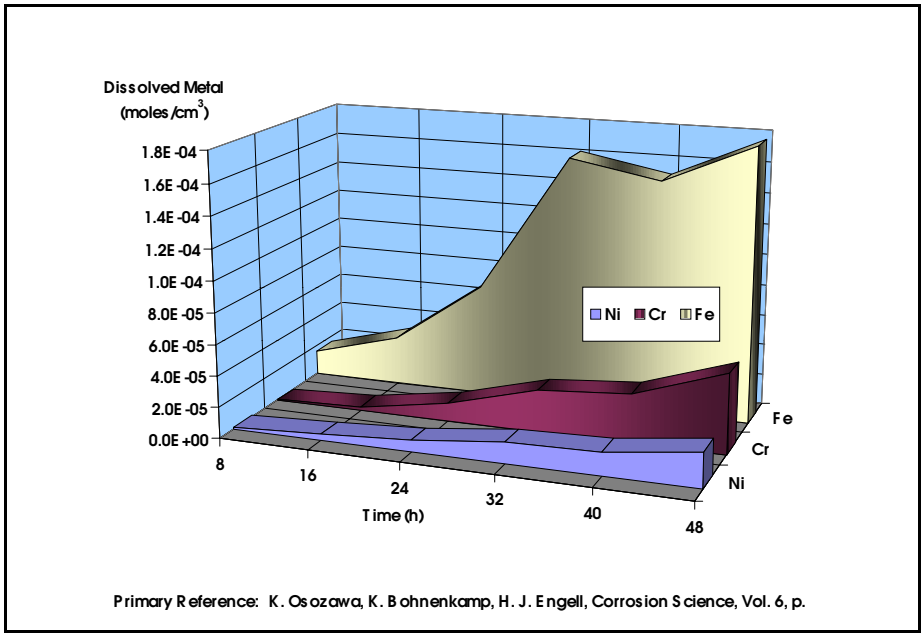

NOTE: Sedriks (p. 184, Fig. 5.7, Ref. 21)

Figure 16. Transient Concentration of Dissolved Metal in Stainless Steel 304 Crevice Exposed to 0.1 N NaCl

6.7.2 Crevice Chemistry and Lowering of Local pH

The hydrolysis of dissolved metal in crevices can lead to the accumulation of H^+ and the corresponding suppression of pH. Metal ions produced by anodic dissolution are assumed to undergo the following hydrolysis reactions, as discussed by Oldfield and Sutton (1978):

$$Fe^{2+} + H_2O \longleftrightarrow Fe(OH)^+ + H^+ \quad \text{(Eq. 18)}$$

$$Fe^{3+} + H_2O \longleftrightarrow Fe(OH)^{2+} + H^+ \quad \text{(Eq. 19)}$$

$$Ni^{2+} + H_2O \longleftrightarrow Ni(OH)^+ + H^+ \quad \text{(Eq. 20)}$$

$$Cr^{3+} + H_2O \longleftrightarrow Cr(OH)^{2+} + H^+ \quad \text{(Eq. 21)}$$

$$Cr(OH)^{2+} + H_2O \longleftrightarrow Cr(OH)_2^+ + H^+ \quad \text{(Eq. 22)}$$

If the dissolved metals exceed the solubility limits, precipitation will occur:

$$Fe(OH)_2(s) \longleftrightarrow Fe^{2+} + 2OH^- \quad \text{(Eq. 23)}$$

$$Ni(OH)_2(s) \longleftrightarrow Ni^{2+} + 2OH^- \quad \text{(Eq. 24)}$$

$$Cr(OH)_3(s) \longleftrightarrow Cr^{3+} + 3OH^- \quad \text{(Eq. 25)}$$

In the case of Stainless steel 316L, the hydrolysis of other dissolved metals such as molybdenum ions may be important.

6.7.3 Chloride Transport by Electromigration

Chloride anion will be driven into the crevice by the potential gradient, as discussed by Xu and Pickering (1993). The corresponding concentration in the crevice is:

$$\left[Cl^-\right] = \left[Cl^-\right]_0 \exp\left[-\frac{F}{RT}\Phi(x)\right] \quad \text{(Eq. 26)}$$

where $[Cl^-]_0$ is the concentration at the crevice mouth, $\Phi(x)$ is the potential in the crevice relative to that at the mouth, and (x) is the distance into the crevice measured from the mouth. Field-driven electromigration of Cl^- (and other anions) into crevice must occur to balance cationic charge associated with H^+ ions and dissolved corrosion products such as Fe^{2+}, Ni^{2+}, and Cr^{3+}. If such conditions do develop inside 316L crevices, LC or SCC might set the stage for accelerated attack of this material.

6.7.4 Deterministic Models of the Crevice

Detailed deterministic models are available in the scientific literature to calculate and compare the spatial distributions of electrochemical potential and current density in WP crevices as well as transient concentration profiles of dissolved metals and ions (Farmer et al. 1998; Farmer and McCright 1998). In this AMR, these quantities are calculated with the transport equations, which govern electromigration, diffusion, and convective transport. In cases with strong supporting electrolyte, electromigration can be ignored (Newman 1991). First, the axial current density along the length of the crevice is calculated by integrating the wall current density. The electrode potential along the length of the crevice can then be calculated from the axial current density. This technique is similar to that employed in other models (Nystrom et al. 1994). Such models show that the electrochemical potential decreases with increasing distance into the crevice. Therefore, the potential should never be more severe (closer to the threshold for LC) than at the crevice mouth. However, the reduced pH and increased Cl- in the occluded cell anode near the crevice mouth (Gartland 1997) reduce the LC threshold ($E_{critical}$). Thus, there is maximum crevice attack at the mouth, as observed. The partial differential equations that define transient concentrations in the crevice require determination of the potential gradient as well as the local generation rates for dissolved species. The concentrations of dissolved metals at the crevice mouth are assumed to be zero. Computations are facilitated by assuming that the crevices are symmetric about a mirror plane where the flux is zero. This model has been used to estimate the extent of pH suppression in WP crevices due to the simultaneous hydrolysis and transport of dissolved Fe, Ni, Cr, Mo, and W.

6.7.5 Experimental Determinations of Crevice pH and Current

The local crevice environments for 316L stainless steel and other relevant alloys are being determined experimentally. This procedure is described in AP-E-20-81. Crevices have been constructed from square metallic samples, 2 inches on each side and 1/8 inch thick (same size as crevice samples used in the LTCTF). The samples are masked with plastic tape, thereby forming an exposed square area, 1.7 inches on each side. The exposed area is placed underneath a clear plastic window with an access port for a pH sensor in the center (inserted through the plastic). In this case, the sensor is miniature reference electrode separated from the crevice solution with a thin glass membrane. A second pH sensor is located at the mouth of the crevice, in close proximity to a saturated calomel reference electrode (SCE). The use of in situ sensors to determine crevice pH has also been described by Sridhar and Dunn (1994). In parallel experiments by Farmer et al. (1998), paper strips with a pH-sensitive dye (pH paper) have been sandwiched between the clear plastic window and photographed with a digital electronic camera in a time-lapse mode to add confidence to the measurements made with pH sensors. Spectroscopic-grade graphite counter electrodes were positioned in the electrolyte just outside the mouth of the crevice. The Ag/AgCl reference electrode was also positioned in the electrolyte just outside the mouth of the crevice. A potentiostat then controlled the electrochemical potential at the mouth of the crevice. Temperature, potential, current, and pH were then recorded electronically during the course of the experiment.

Measurements of pH and current inside crevices formed from 316L stainless steel are shown in Figures 17 through 20. The electrolyte was 4M NaCl and was maintained at ambient temperature. Since this electrolyte contains no buffer ions, it is considered to be a far more

severe medium than those representative of various concentrations of J-13 well water. In the first case, represented by Figures 17 and 18, the electrochemical potential at the mouth was maintained at 200 mV versus Ag/AgCl. Crevice corrosion could be seen initiating near the crevice mouth and propagating towards the pH sensor, which was located about 0.5 cm inside the crevice mouth. When the corrosion front reaches the pH sensor, the pH dropped from the initial value (pH~7) to a very low value (pH~1). The fixed one-liter volume of electrolyte outside of the crevice became slightly alkaline. The pH of this solution reached a maximum (pH~10) and then fell to a slightly lower steady-state value (pH~9). Active corrosion inside the crevice is evident since the color of the crevice solution becomes emerald green. Essentially the same results were obtained at 400 mV, as illustrated by Figures 19 and 20. Pits have been observed to initiate inside the crevice. In similar experiments with 316L exposed to SCW, no significant lowering of the pH and no crevice corrosion was observed (CRWMS M&O 2000d). This promising result indicates that ground waters at Yucca Mountain may inhibit LC.

In summary, the current density and imposed electric field within the crevice was sufficient to cause significant acidification. In many of the experiments described here, both the applied potential and the test medium are more severe than those expected in the repository. However, the temperature of aqueous solutions on the WP surface may be significantly higher (120°C). Work is in progress to obtain comparable data at higher temperature. Based upon experimental work with 316L crevices without buffer, it is believed an increase in potential to 200 mV versus Ag/AgCl at the mouth of the crevice can lead to a pH as low as approximately one (~1). In the actual WP system, such an increase in potential at the crevice mouth will only be possible in cases with extreme gamma radiolysis or microbial activity.

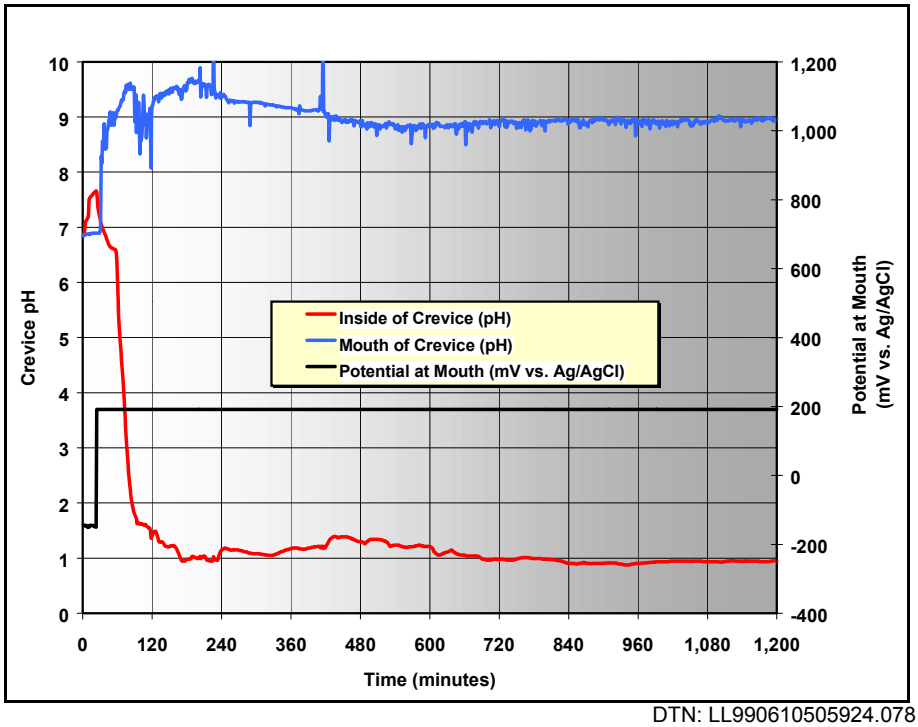

DTN: LL990610505924.078

Figure 17. Stainless Steel 316L, 4M NaCl, 200 mV and 23°C, Crevice pH versus Time

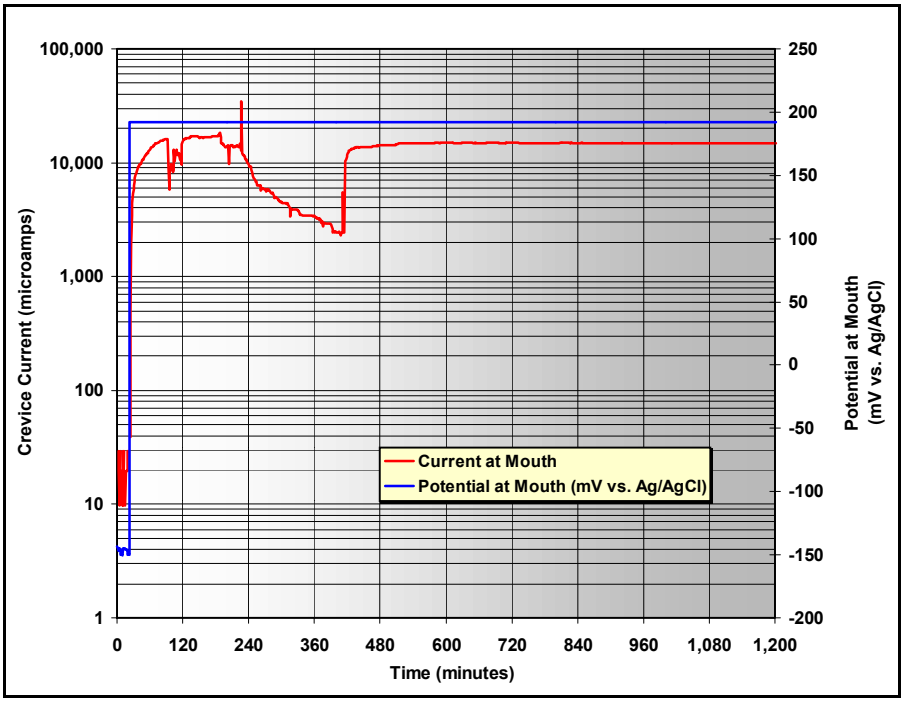

DTN: LL990610505924.078

Figure 18. Stainless Steel 316L, 4M NaCl, 200 mV and 23°C, Crevice Current versus Time

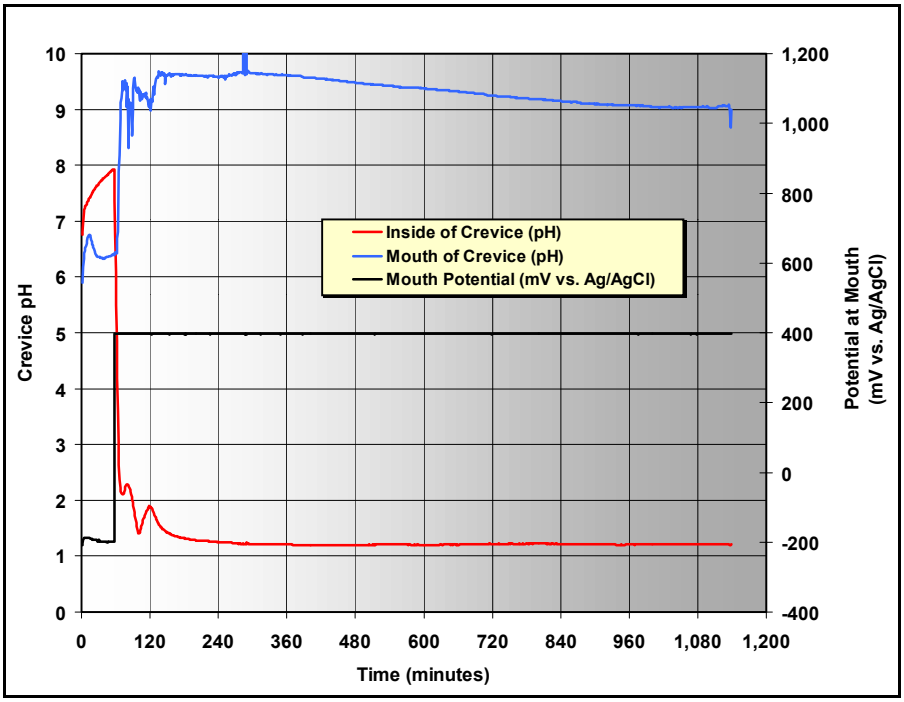

DTN: LL990610505924.078

Figure 19. Stainless Steel 316L, 4M NaCl, 400 mV and 23°C, Crevice pH versus Time

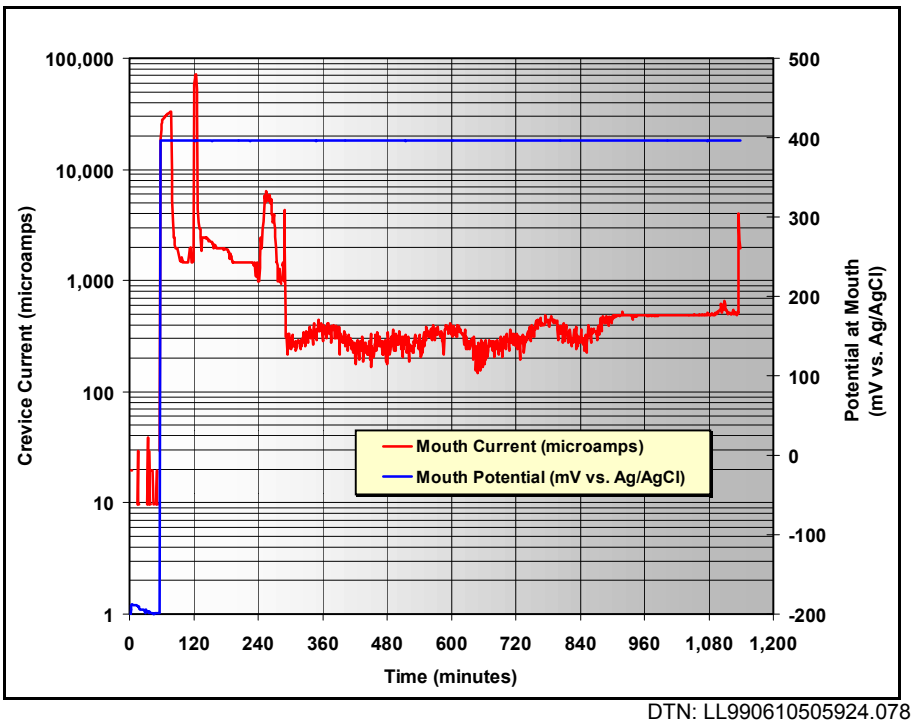

DTN: LL990610505924.078

Figure 20. Stainless Steel 316L, 4M NaCl, 400 mV and 23°C, Crevice pH versus Time

6.8 EFFECTS OF SENSITIZATION AND THERMAL AGING ON CORROSION

The effect of thermal aging on the corrosion rate is accounted for in an enhancement factor, G_{aged}, and is based upon a ratio of the non-equilibrium current densities for base metal and aged material.

$$\left.\frac{dp}{dt}\right|_{effective} = G_{aged} \times \left.\frac{dp}{dt}\right|_{effective} \qquad \text{(Eq. 27)}$$

The value of G_{aged} for base metal is approximately one ($G_{aged} \sim 1$), whereas the value of G_{aged} for fully aged material is larger ($G_{aged} \sim 10$). Material with less precipitation than the fully aged material would have an intermediate value of G_{aged} ($1 \leq G_{aged} \leq 10$).

The most useful method of determining the stability of a particular alloy is to complete a precipitation study (Gdowski and Bullen 1988, p. 15). TTP diagrams indicate the conditions required for precipitation of equilibrium phases to be formed. Precipitation in Type 304 stainless steel has been adequately described since $M_{23}C_6$ is the predominant precipitate phase (Gdowski and Bullen 1988). The TTP diagrams for Type 316 stainless steel are more complicated. In aging studies conducted at 816°C for up to 10,000 hours, the $M_{23}C_6$ concentration increases almost immediately. The chi (χ) phase begins to precipitate at about 150 hours, while the sigma (σ) and Laves phases do not begin to precipitate until about 500 and 1000 hours, respectively. By lowering the carbon content of Type 316 stainless steel to a level corresponding to Type 316L, the time required for formation of a given quantity of $M_{23}C_6$ is

significantly lengthened. After the precipitated carbide phase reaches a maximum, it can begin to redissolve into the bulk. The formation of both $M_{23}C_6$ and sigma phases are accelerated by cold working.

Precipitate formations in Types 304L and 316L stainless steels have a significant impact on the mechanical properties and corrosion resistance of these materials. Studies indicate that these alloys can undergo significant microstructural evolution at moderate temperature ($T < 650°C$) over relatively short times ($t < 1000$ hours). Repository temperature, though considerably lower ($T < 250°C$) could promote precipitation in the time period of interest for container retrieval ($t < 450{,}000$ hours). Studies of long-term, low-temperature phase stability or computer modeling of the diffusion of precipitate constituents may be required to determine the potential use of Types 304L and 316L stainless steels as container materials.

Intergranular SCC and LC occur when these materials are subjected to a sufficiently severe combination of sensitization, corrosive environment, and stress (Farmer et al. 1988, pp. 44-45). Sensitization is a term denoting increased susceptibility to attack following a thermal exposure that causes chromium-rich $M_{23}C_6$ carbides to precipitate at grain boundaries. The subject of sensitization has been the subject of extensive investigation. Chromium carbide precipitation in stainless steels occurs in the temperature range from 500 to 850°C (930 to 1560°F) with the rate of precipitation controlled by chromium diffusion. A variety of metallurgical changes have been suggested as mechanisms for sensitization, but it is generally accepted that the principal feature responsible is a narrow chromium-depleted zone adjacent to the carbides. It is generally accepted that susceptibility to intergranular attack occurs when there is an essentially continuous zone in which the local chromium concentration is below about 13 atomic percent. Chromium is the element responsible for the formation of stable passive films on stainless steels, and localized depletion of this element adjacent to grain boundaries results in the establishment of an active path (one which does not readily repassivate) into the bulk material. The width of this chromium-depleted region is typically 200 nm (Sedriks 1996, p. 232, Fig. 6.2).

The austenite chromium concentration in equilibrium with the $Cr_{23}C_6$ carbide depends most sensitively on the activity coefficient of chromium and on the activity of carbon, as expected from thermodynamic arguments (Sedriks 1996, pp. 245-249). It is assumed that the diffusing chromium atom reacts with a coordinated carbon atom. Therefore, decreasing the carbon content can lower susceptibility to sensitization. Additions of titanium and niobium, which are both strong carbide formers, can also lower susceptibility to sensitization.

The low-temperature sensitization of stainless steels has also been studied. It has been concluded that nitrogen additions up to 0.14% are not detrimental to intergranular corrosion resistance. Sensitization could not be induced, provided that the carbon content was maintained below 0.02%.

The sensitization of Type 304 stainless steel heated for 2 hours at 650°C has been studied by exposing samples to boiling nitric acid (Huey Test, ASTM A262-98, 1999, Practice C). Results show that sensitization is kept to an insignificant level as long as the carbon content is

maintained below 0.03 weight percent. At carbon contents greater than 0.03 wt.%, there is a rapid increase in corrosion rate.

Molybdenum at the 2 to 3 wt.% level in 316 stainless steel has been previously regarded as detrimental to intergranular corrosion resistance. In the Huey Test, high rates of intergranular attack are observed in sensitized Type 316 even at carbon contents below the maximum specified for the L grade. Current thinking is that these high rates of attack are peculiar to the Huey Test, which attacks a number of phases in addition to chromium-depleted regions. In tests with solutions of copper sulfate in sulfuric acid (ASTM A262-98, 1999, Practice E), the presence of 2 wt.% molybdenum actually reduces the tendency to sensitization. The reason for the high rates of attack observed in Type 316L in the Huey Test has never been conclusively established. Since molybdenum favors the formation of the sigma phase, this effect has been attributed to the presence of sub-microscopic sigma phase. It has been noted that aside from the Huey test, sub-microscopic sigma is known to have caused intergranular attack only in one other environment, 25% H_2SO4 at 40°C. Sigma, when present as an identifiable phases at grain boundaries, causes intergranular corrosion in the Huey test and hence should be avoided in stainless steels used for nitric acid service. However, molybdenum-containing 316L is not usually selected for nitric acid service because Type 304L exhibits better corrosion resistance and is less expensive.

Electrochemical Potentiokinetic Reactivation (EPR) is used as a means of measuring the anodic dissolution of sensitized regions of stainless steels (Sedriks 1996, pp. 239-242). The single-loop EPR has been standardized as ASTM G108-94, 1999. For example, Type 304 or 304L stainless steel sample is polished with 1 micron diamond paste and polarized in an electrolyte that consists of 0.5 M H_2SO_4 with 0.01 M KSCN at 30°C. After establishing E_{corr} for about 2 minutes, the potential of the specimen is raised to 200 mV versus SCE for an additional 2 minutes, thereby passivating the entire surface. The potential is then gradually returned to E_{corr} at a rate of 6 volts per hour. This decrease results in reactivation of the specimen, which involves preferential breakdown of the passive film covering the chromium-depleted regions of the material. Consequently, a large anodic peak is generated in the potential verses current curve. The charge is calculated by integrating the area underneath this peak. The grain boundary area can then be estimated with the following equations. The total active grain boundary area (cm^2) is calculated as:

$$X = A_S(5.1\times10^{-3}e^{0.35}G) \qquad \text{(Eq. 28)}$$

where A_S is the specimen area (cm^2), and G is the grain size at a magnification of ×100 measured in accordance with ASTM Test Method E 112-96, 1996. It is assumed that the corrosive attack is restricted to the grain boudaries, that the attack is distributed uniformly over the entire grain boundary area, and that the width of the attacked grain boundary is 10^{-4} cm (different than that quoted above). Having a value for the total active grain boundary area, X, enables the electrochemically-measured charge in coulombs, Q, to be normailized to a value that is approximately independent of grain size using the equation:

$$P_a = \frac{Q}{X} \qquad \text{(Eq. 29)}$$

where P_a is the normailized charge (or current density) in coulombs per square centimeter. The height of anodic peaks are used as an approximate measure of the integrated charge underneath the corresponding peaks. It is assumed that Q is proportional to peak height in double-loop EPR.

Anodic polarization curves also show that the non-equilibrium passive current density (corrosion rate) increases with the extent of sensitization (Sedriks 1996, p. 240, Fig. 6.5). Type 304 stainless steel sensitized for 1000 hours at 650°C exhibits a peak current density of approximately 2×10^4 μA cm^{-2} in 2N H_2SO_4 at 90°C and 0 mV versus NHE. Under comparable conditions, non-sensitized samples exhibited a peak current density of approximately 2×10^3 μA cm^{-2}. Since the distribution of this current density over the sample surface is unknown, it is difficult to convert these current densities into actual penetration rates. If it is assumed that all of the current density is attributable to the chromium-depleted grain boundaries (similar to assumptions used in EPR), it can also be assumed that the rate of intergranular penetration is increased by a factor of ten (×10) by full sensitization. This corresponds to a case where G_{aged} is approximately ten ($G_{aged} \sim 10$) at chromium-depleted grain boundaries. Here it is assumed that these depleted regions are about 200 nm wide ($\delta = 2\times10^{-5}$ cm). Assuming a circular grain with a diameter D, the fraction of the grain depleted in chromium is then:

$$\theta_{GB} = 1 - \frac{D^2}{(D+\delta)^2} \qquad \text{(Eq. 30)}$$

This is the fraction of the exposed surface that would experience a corrosion rate enhancement characterized by the factor G_{aged}. Alternatively, LC rates could be applied to the fraction of the area represented by θ_{GB}, with GC rates applied to the remaining area.

6.9 MICROBIALLY INFLUENCED CORROSION

It has been observed that stainless steels such as 316NG are susceptible to MIC (Lian et al. 1999). Furthermore, it is believed that microbial growth in the repository will be limited by the availability of nutrients. For example, H^+ is known to be generated by bacterial isolates from Yucca Mountain. Furthermore, thiobaccilus ferrooxidans oxidize Fe^{2+} while geobacter metallireducens reduce Fe^{3+}. Other microbes can reduce SO_4^{2-} and produce S^{2-}. Ultimately, the impact of MIC will be accounted for by adjusting E_{corr}, $E_{critical}$, pH, and the sulfide concentration. The possible acceleration of abiotic corrosion processes by microbial growth is addressed here. Lian et al. (1999) have shown that MIC can enhance corrosion rates of 304 stainless steel by a factor of approximately ten (×10). Measurements for 304 stainless steel and other similar materials are shown in Table 12. Figure 21 is a schematic representation of the corrosion model for the 316NG structural support. MIC enhances corrosion rates as shown in Figure 21. In this illustration G_{MIC} is the enhancement factor.

$$\left.\frac{dp}{dt}\right|_{effective} = G_{MIC} \times \left.\frac{dp}{dt}\right|_{effective} \qquad \text{(Eq. 31)}$$

This factor is calculated as the ratio of corrosion rates (microbes to sterile) and from Table 12. The value of G_{aged} for 304 stainless steel in sterile media is approximately one ($G_{MIC} \sim 1$), whereas the value of G_{aged} for 304 stainless steel in innoculated media is larger ($G_{aged} \sim 10$). It is assumed that MIC will have the same effect on 316NG stainless steel.

The principal nutrient-limiting factor to microbial growth in situ at Yucca Mountain (YM) has been determined to be low levels of phosphate. There is virtually no phosphate contained in J-13 groundwater. YM bacteria grown in the presence of YM tuff are apparently able to solubilize phosphate contained in the tuff to support growth to levels of 10^6 cells ml^{-1} of groundwater. When exogenous phosphate is added (10 mM), then levels of bacterial growth increase to 10^7 to10^8 cells ml^{-1}. The 1 to 2 orders-of-magnitude difference in bacterial growth with and without the presence of exogenous phosphate is almost certainly not significant with respect to effects on corrosion rates. Therefore, nutrient limitation at least at a first approximation was not factored into the overall MIC model. It may be noted, however, that the 10-fold G_{MIC} included in the model was in the presence of sufficient phosphate to sustain higher levels of bacterial growth (in an effort to achieve accelerated conditions).

Other environmental factors that could effect levels of bacterial growth include temperature and radiation. These factors, however, are closely coupled to RH; as temperature and radiation decrease in the repository, RH is predicted to increase. At the same time, while there are some types of microorganisms that can survive elevated temperatures ($\leq 120^oC$) and high radiation doses, if there is no available water, then bacterial activity is completely prevented. Thus, because water availability is the primary limiting factor and this factor is coupled to other less critical limiting factors, water availability (as expressed by RH) was used as the primary gauge of microbial activity.

Determination of a critical mass of *total* bacteria required to cause MIC is not an issue that needs to be addressed in the MIC model. Bacterial densities in YM rock have been determined to be on the order of 10^4 to 10^5 cells gm^{-1} of rock. In absolute terms, this is almost certainly above the threshold required to cause MIC. Further, bacterial densities were shown to increase 1 to 2 orders-of-magnitude when water is available (above). A more germane concern is the types of bacteria present, their abundance, and how their relative numbers are affected when water is available for growth. Corrosion rates will be affected (at least on some WP materials), for example, if organic acid producers out compete sulfate reducers or inorganic acid producers for available nutrients when water is sufficient to support growth. No data is currently available regarding the composition of the bacterial community over the changing environmental conditions anticipated during repository evolution. Instead, this issue has been addressed in the current model by determining overall corrosion rates under a standardized set of conditions, in the presence and absence of a defined set of characterized YM bacteria. Clearly, more data is required to better predict MIC on any given material with respect to this concern. Corrosion rates are currently being determined in the presence of YM rock containing the complete complement of YM bacteria and under conditions more representative of the repository.

MIC is defined as a localized effect; thus, not all areas are equivalent on any given WP with respect to bacterial colonization. It is well documented that bacteria preferentially colonize

weldments, heat-affected zones, and charged regions (Borenstein and White 1989; Walsh 1999; Enos and Taylor 1996). However, the current model is based on data collected using unwelded specimens. In order to account for preferential areas of colonization in the model, it might be assumed that G_{MIC} is uniformly distributed with respect to area distribution.

Table 12. Impact of MIC on Corrosion of WP Materials

Tested Sample Initial Condition	Average Corrosion Rate (μm/yr)	Corrosion Potential E_{corr} (V vs SCE)	
		Initial	Endpoint
CS1020 + YM Microbes	8.8	-0.660	-0.685
Sterile CS 1020	1.4	-0.500	-0.550
M400 + YM Microbes	1.02	-0.415	-0.315
Sterile M400	0.005	-0.135	-0.070
C-22 + YM Microbes	0.022	-0.440	-0.252
Sterile C-22	0.011	-0.260	-0.200
I625 + YM Microbes	0.013	-0.440	-0.285
Sterile I625	0.003	-0.160	-0.130
304SS + YM Microbes	0.035	-0.540	-0.280
Sterile 304SS	0.003	-0.145	-0.065

DTN: LL991203505924.094

NOTE: Horn et al. (1999)

6.10 MODEL VALIDATION

Model validation in this AMR has been accomplished following the guidelines cited in ASTM C 1174, 1997 (Sections 13.2, 14.1.5, 14.2, 20.4). According to ASTM C 1174 (Section 20.4.3.1), validation of the model means the model can account for all available data. In this AMR, data obtained from simulated laboratory scale experiments have been used along with published data to test well-known mathematical models available in the scientific literature on the corrosion of stainless steels.

Statistical analyses performed using data sets contained in this AMR showed excellent correlation between the experimental data and the values predicted by the model. This is evident from the high values predicted by the model. This is evident from the high value of correlation coefficients (e.g., $R > 0.9$). Consequently, predictions (e.g., corrosion rates, corrosion potentials, etc.) based on the models used in this AMR are all valid.

6.11 SUMMARY OF MODEL

The model for the general and LC of stainless steel 316NG or 316L is summarized in Figure 1. First, any corrosion of the structural support requires penetration of the WPOB. The threshold RH represented by Figure 2 and Equation 1 is first used to determine whether or not DOX will take place. If dry oxidation is determined to occur, the parabolic growth law represented by Equations 6 through 12 is then used to calculate the corrosion rate as a function of temperature. If the threshold RH is exceeded, HAC will occur in the absence of dripping water, and APC will occur in the presence of dripping water. If APC is assumed to occur, the corrosion and critical potentials are used to determine whether the mode of attack is general or localized. The

correlations represented by Equation 16 and Table 4 are used as the basis for estimating these potentials at the 50th percentile. Since the material specifications will be based partly on the measured corrosion and critical potentials, it will be assumed that these potentials will be uniformly distributed about the 50th percentile values determined from the correlation. For example, the 0th and 100th percentile values of E_{corr} will be assumed to be at E_{corr} (50th percentile) ± ΔE_{corr}. Similarly, the 0th and 100th percentile values of $E_{critical}$ will be assumed to be at $E_{critical}$ (50th percentile) ± $\Delta E_{critical}$. The desired values for ΔE_{corr} and $\Delta E_{critical}$ can be determined by inspecting Table 5. Values ranging from 25 to 75 mV seem like reasonable choices, based upon SSW. Alloy heats would be tested before use with any materials falling outside of the specified range being rejected. If the comparison of E_{corr} to $E_{critical}$ indicates GC, the distribution of rates determined from Figures 11 and 12 will be used as the basis of the general and localized rates of corrosion. This model does not yet account for the effects of aging and sensitization on corrosion rates. However, such enhancements of the corrosion rate will be accounted for in the future.

The effects of MIC and aging can be accounted for through the strategy shown in Figure 21 (only illustrated with G_{MIC}). Sensitization is a term denoting increased susceptibility to attack following a thermal exposure that causes chromium-rich $M_{23}C_6$ carbides to precipitate at grain boundaries. The subject of sensitization has been the subject of extensive investigation. Chromium carbide precipitation in stainless steels occurs in the temperature range from 500 to 850°C (930 to 1560°F), with the rate of precipitation controlled by chromium diffusion. A variety of metallurgical changes have been suggested as mechanisms for sensitization, but it is generally accepted that the principal feature responsible is a narrow chromium-depleted zone adjacent to the carbides. It is generally accepted that susceptibility to intergranular attack occurs when there is an essentially continuous zone in which the local chromium concentration is below about 13 atomic percent. Chromium is the element responsible for the formation of stable passive films on stainless steels, and localized depletion of this element adjacent to grain boundaries results in the establishment of an active path (one which does not readily repassivate) into the bulk material. The width of this chromium-depleted region is typically 200 nm. The effect of thermal aging on the corrosion rate is accounted for in an enhancement factor for sensitized grain boundaries (G_{aged}). In the case of non-sensitized base metal, this enhancement factor is unity ($G_{aged} \sim 1$), whereas the value for completely sensitized grain boundary is much larger ($G_{aged} \sim 10$). Material with less carbide precipitation than the fully sensitized material would have an intermediate value of G_{aged} ($1 \leq G_{aged} \leq 10$). Here it is assumed that these depleted regions are about 200 nm wide ($\delta = 2\times10^{-5}$ cm). The fraction falling within the chromium-depleted region would experience corrosion rate enhancement ($G_{aged} \geq 1$). Alternatively, LC rates could be applied to the fraction of the area represented by θ_{GB}, with GC rates applied to the remaining area.

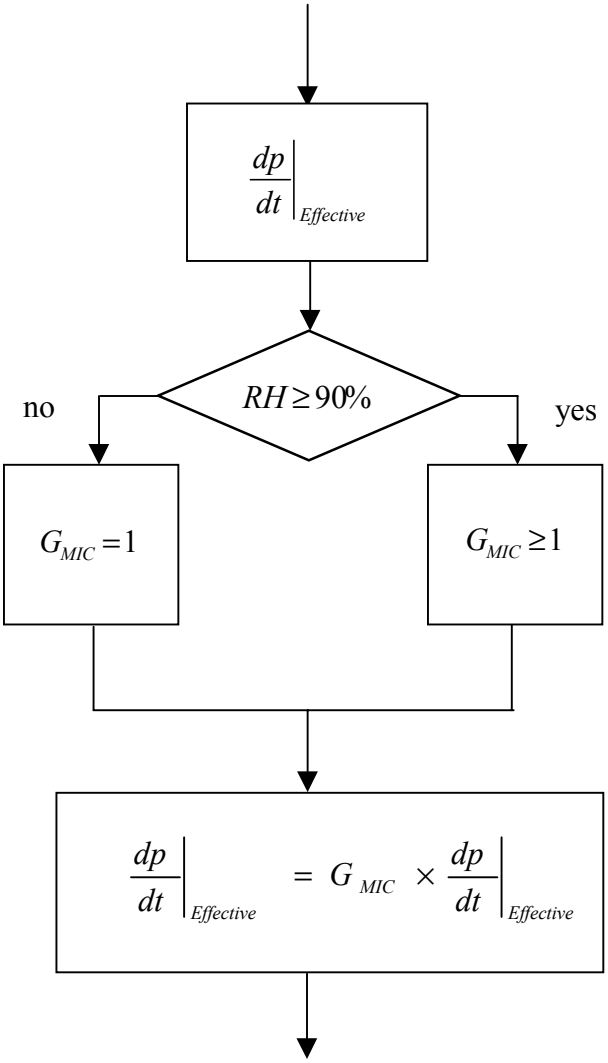

Figure 21. Schematic Representation Showing Augmentation of Model to Account for MIC

7. CONCLUSIONS

A model for corrosive degradation of the 316NG structural support has been developed. This model uses threshold RH to determine whether or not DOX or HAC will occur. If conditions for HAC exist, in conjunction with dripping, APC can occur. If APC can occur, a comparison of the threshold potential to the corrosion potential is used as the basis for determining whether or not LC will occur. Both general and local corrosion rates are determined from the distributions based upon a broad range of published literature data. An apparent activation energy is estimated from scant data to enable scaling of rates with temperature, if desired. Most of the available data was obtained at ambient temperature.

This document and its conclusions may be affected by technical product input information that requires confirmation. Any changes to the document that may occur as a result of completing the confirmation activities will be reflected in subsequent revisions. The status of the input information quality may be confirmed by review of the Document Input Reference System Database.

The following data tracking numbers (DTNs) have been assigned to the data developed in this AMR:

- DTN: LL990610105924.074
- DTN: LL990610505924.078
- DTN: LL991203505924.094
- DTN: LL991208205924.096
- DTN: LL991210205924.104
- DTN: LL991210305924.105
- DTN: LL991210405924.107
- DTN: LL000201505924.122.

8. INPUTS AND REFERENCES

8.1 DOCUMENTS CITED

Andresen, P.L. 1988. "Modeling of Water and Material Chemistry Effects on Crack Tip Chemistry and Resulting Crack Growth Kinetics." *Proceedings of the Third International Symposium on Environmental Degradation of Materials in Nuclear Power Systems-Water Reactors held August 30-September 3, 1987 in Traverse City, Michigan.* 301-312. Warrendale, Pennsylvania: The Metallurgical Society. TIC: 246608.

Bard, A.J. and Faulkner, L.R. 1980. "Liquid Junction Potentials." Section 2.3 of *Electrochemical Methods, Fundamentals and Applications.* New York, New York: John Wiley & Sons. TIC: 245183.

Borenstein, S.W. and White, D.C. 1989. "Influence of Welding Variables on Microbiologically Influenced Corrosion of Austenitic Stainless Steel Weldments." *Corrosion 89 April-17-21, 1989 New Orleans Convention Center, New Orleans, Louisiana, Paper Number 183,* 183/1 - 183/13. Houston, Texas: National Association of Corrosion Engineers. TIC: 246583.

CRWMS M&O (Civilian Radioactive Waste Management System Management and Operating Contractor) 1999a. *Monitored Geologic Repository Project Description Document.* B00000000-01717-1705-00003. Las Vegas, Nevada: CRWMS M&O. ACC: MOL.19991117.0160.

CRWMS M&O 1999b. *General Corrosion and Localized Corrosion of Waste Package Outer Barrier.* Work Direction and Planning Document. Las Vegas, Nevada: CRWMS M&O. ACC: MOL.19990708.0230.

CRWMS M&O 1999c. *Classification of the MGR Uncanistered Spent Nuclear Fuel Disposal Container System.* ANL-UDC-SE-000001 REV 00. Las Vegas, Nevada: CRWMS M&O. ACC: MOL.19990928.0216.

CRWMS M&O 1999d. *11017040 Long Term Materials Testing and Modeling.* Activity Evaluation. Las Vegas, Nevada: CRWMS M&O. ACC: MOL.19990224.0429.

CRWMS M&O 1999e. *Waste Package Materials Properties.* BBA000000-01717-0210-00017 REV 00. Las Vegas, Nevada: CRWMS M&O. ACC: MOL.19990407.0172.

CRWMS M&O 1999f. *Uncanistered Spent Nuclear Fuel Disposal Container System Description Document.* SDD-UDC-SE-000001 REV 00. Las Vegas, Nevada: CRWMS M&O. ACC: MOL.19991217.0512.

CRWMS M&O 2000a. *Environment on the Surfaces of the Drip Shield and Waste Package Outer Barrier.* Input Transmittal WP-LNL-00018.T. Las Vegas, Nevada: CRWMS M&O. ACC: MOL.20000118.0316.

CRWMS M&O 2000b. *Aging and Phase Stability of Waste Package Outer Barrier Model.* Input Transmittal WP-LNL-00019.T. Las Vegas, Nevada: CRWMS M&O. ACC: MOL.20000118.0317.

CRWMS M&O 2000c *General Corrosion and Localized Corrosion of the Drip Shield.* Input Transmittal WP-LNL-00022.T. Las Vegas, Nevada: CRWMS M&O. ACC: MOL.20000118.0318.

CRWMS M&O 2000d. *General Corrosion and Localized Corrosion of Waste Package Outer Barrier.* ANL-EBS-MD-000003 REV 00. Las Vegas, Nevada: CRWMS M&O. ACC: MOL.20000202.0172.

DOE (U.S. Department of Energy) 2000. *Quality Assurance Requirements and Description.* DOE/RW-0333P, Rev. 9. Washington, D.C.: U.S. Department of Energy, Office of Civilian Radioactive Waste Management. ACC: MOL.19991028.0012.

Enos, D.G. and Taylor, S.R. 1996. "Influence of Sulfate-Reducing Bacteria on Alloy 625 and Austenitic Stainless Steel Weldments." *Corrosion Science, 52,* (11), 831-843. Houston, Texas: National Association of Corrosion Engineers International. TIC: 246554.

Estill, J.C. 1998. "Long-Term Corrosion Studies ." 2.2 of *Engineered Materials Characterization Report.* McCright, R.D., ed. UCRL-ID-119564 Volume 3 Rev.1.1. Livermore, California: Lawrence Livermore National Laboratory. ACC: MOL.19981222.0137.

Farmer, J.C. and McCright, R.D. 1998. "Crevice Corrosion and Pitting of High-Level Waste Containers: Integration of Deterministic and Probabilistic Models." *Proceedings of Corrosion 98, March 22-27, 1998, San Diego, California.* 160/1 to 160/24. Houston, Texas: NACE International. TIC: 238172.

Farmer, J.C.; McCright, R.D.; Estill, J.C.; and Gordon, S.R. 1998. *Development of Integrated Mechanistically-Based Degradation-Mode Models for Performance Assessment of High-Level Waste Containers.* URCL-JC-130811, Rev. 1. Livermore, California: Lawrence Livermore National Laboratory. ACC: MOL.19990729.0007.

Farmer, J.C.; McCright, R.D.; Estill, J.C.; and Gordon, S.R. 1999. "Development of Integrated Mechanistically-Based Degradation-Mode Models for Performance Assessment of High-Level Waste Containers." *Scientific Basis for Nuclear Waste Management XXII, Symposium held November 30-December 4, 1998, Boston, Massachusetts, U.S.A.* Wronkiewicz, D.J. and Lee, J.H., eds. *556,* 855-862. Warrendale, Pennsylvania: Materials Research Society. TIC: 246426.

Farmer, J.C.; Van Konynenburg, R.A.; McCright, R.D.; and Bullen, D.B. 1988. *Localized Corrosion and Stress Corrosion Cracking of Austenitic Steels.* Volume 3 of *Survey of Degradation Modes of Candidate Materials for High-Level Radioactive-Waste Disposal Containers.* UCID-21362. Livermore, California: Lawrence Livermore National Laboratory. ACC: MOL.19980715.0385.

Gartland, P.O. 1997. "A Simple Model of Crevice Corrosion Propagation for Stainless Steels in Seawater." *Corrosion 97.* 417/1 to 417/17. Houston, Texas: NACE International. TIC: 245216.

Gdowski, G.E. and Bullen, D.B. 1988. *Oxidation and Corrosion.* Volume 2 of *Survey Of Degradation Modes of Candidate Materials for High-Level Radioactive-Waste Disposal Containers.* UCID-21362. Livermore, California: Lawrence Livermore National Laboratory. ACC: MOL.19980715.0384.

Glass, R.S.; Overturf, G.E.; Van Konynenburg, R.A.; and McCright, R.D. 1986. "Gamma Radiation Effects on Corrosion-I. Electrochemical Mechanisms for the Aqueous Corrosion Processes of Austenitic Stainless Steels Relevant to Nuclear Waste Disposal in Tuff." *Corrosion Science, 26,* (8), 577-590. Oxford, Great Britain: Pergamon. TIC: 226179.

Gruss, K.A.; Cragnolino, G.A.; Dunn, D.S.; and Sridhar, N. 1998. "Repassivation Potential for Localized Corrosion of Alloys 625 and C22 in Simulated Repository Environments." *Proceedings of Corrosion 98, March 22-27, 1998, San Diego, California.* 149/1 to 149/15. Houston, Texas: NACE International. TIC: 237149.

Hack, H.P. 1983. "Crevice Corrosion Behavior of Molybdenum-Containing Stainless Steels in Seawater." *Materials Performance, 22,* (6), 24-30. Houston, Texas: NACE International. TIC: 245826.

Harrar, J.E.; Carley, J.F.; Isherwood, W.F.; and Raber, E. 1990. *Report of the Committee to Review the Use of J-13 Well Water in Nevada Nuclear Waste Storage Investigations.* UCID-21867. Livermore, California: Lawrence Livermore National Laboratory. ACC: NNA.19910131.0274.

Horn, J.M.; Rivera, A.; Lian, T.; and Jones, D. 1998. "MIC Evaluation and Testing for the Yucca Mountain Repository." *Proceedings of Corrosion 98, National Association of Corrosion Engineers, March 22-27, San Diego, California.* 152/2 to 152/14. Houston, Texas: NACE International. TIC: 237146.

Jones, D.A. 1996. Principles and Prevention of Corrosion. 2nd Edition. Upper Saddle River, New Jersey: Prentice Hall. TIC: 241233

Kim, Y.J. 1987. "Effect of Gamma Radiation on Electrochemical Behavior of 9 Cr-1Mo Alloy in NaCl Solutions." *Journal of the Corrosion Science Society of Korea, 16,* (1), 25-30. Seoul, Korea: Corrosion Science Society of Korea. TIC: 246337.

Kim, Y-K. 1988. "Electrochemical Mechanisms for Radiation Corrosion Processes of 316 Austenitic Stainless Steel in Chloride Environment." *Journal of the Corrosion Science Society of Korea, 17,* (1), 20-26. Seoul, Korea: Korean Corrosion Science Society. TIC: 246622.

Kim, Y- K. 1999a. "Analysis of Oxide Film Formed on Type 304 Stainless Steel in 288°C Water Containing Oxygen, Hydrogen, and Hydrogen Peroxide." *Corrosion, 55,* (1), 81-88. Houston, Texas: NACE International. TIC: 245184.

Kim, Y- K. 1999b. "In-Situ Electrochemical Impedance Measurement of Oxide Film on 304 SS in 288°C Water." *Corrosion 99. Paper No. 437,* 1-11. Houston, Texas: NACE International. TIC: 246024.

Leygraf, C. 1995. "Atmospheric Corrosion." Chapter 12 of *Corrosion Mechanisms in Theory and Practice.* Marcus, P. and Oudar, J., eds. New York, New York: Marcel Dekker. TIC: 104415.

Lian, T.; Martin, S.; Jones, D.; Rivera, A.; and Horn, J. 1999. "Corrosion of Candidate Container Materials by Yucca Mountain Bacteria." *Corrosion 99. Paper No. 476,* Houston, Texas: NACE International. TIC: 245833.

Newman, J.S. 1991. "Infinitely Dilute Solutions." *Electrochemical Systems, 2nd Edition.* Section 11.5. 250-251. Englewood Cliffs, New Jersey: Prentice Hall. TIC: 245901.

Nystrom, E.A.; Lee, J.B.; Sagues, A.A.; and Pickering, H.W. 1994. "An Approach for Estimating Anodic Current Distributions in Crevice Corrosion from Potential Measurements." *Journal of the Electrochemical Society, 141,* (2), 358-361. Pennington, New Jersey: Electrochemical Society. TIC: 236472.

Oldfield, J.W. and Sutton, W.H. 1978. "Crevice Corrosion of Stainless Steels. I. A Mathematical Model." *British Corrosion Journal, 13,* (1), 13-22. London, England: Institute of Materials. TIC: 212461.

Pourbaix, M. 1974. *Atlas of Electrochemical Equilibria in Aqueous Solutions.* 644. Houston, Texas: National Association of Corrosion Engineers. TIC: 208955.

Scully, J.R.; Hudson, J.L.; Lunt, T.; Ilevbare, G.; and Kehler, B. 1999. *Localized Corrosion Initiation and Transition to Stabilization in Alloys 625 and C-22.* Charlottesville, Virginia: University of Virginia. TIC: 246630.

Sedriks, A.J. 1996. *Corrosion of Stainless Steels.* 2nd Edition. 179, 377. New York, New York: John Wiley & Sons. TIC: 245121.

Sridhar, N. and Dunn, D.S. 1994. "Effect of Applied Potential on Changes in Solution Chemistry Inside Crevices on Type 304L Stainless Steel and Alloy 825." *Corrosion, 50,* (11), 857-872. Houston, Texas: National Association of Corrosion Engineers International. TIC: 245832.

Walsh, D.W. 1999. "The Effects of Microstructure on MIC Susceptibility in High Strength Aluminum Alloys." *Corrosion 99. Paper No. 187,* 1-13. Houston, Texas: NACE International. TIC: 246549.

Walton, J.C.; Cragnolino, G.; and Kalandros, S.K. 1996. "A Numerical Model of Crevice Corrosion for Passive and Active Metals." *Corrosion Science, 38,* (1), 1-18. Amsterdam, The Netherlands: Pergamon. TIC: 233439.

Welsch, G.; Smialek, J.L.; Doychak, J.; Waldman, J.; and Jacobson, N.S. 1996. "High Temperature Oxidation and Properties." Chapter 2 of *Oxidation and Corrosion of Intermetallic Alloys.* Welsch, G. and Desai, P.D.; eds. West Lafayette, Indiana: Purdue University. TIC: 245280.

Xu, Y. and Pickering, H.W. 1993. "The Initial Potential and Current Distributions of the Crevice Corrosion Process." *Journal of the Electrochemical Society, 140,* (3), 658-668. Pennington, New Jersey: Electrochemical Society. TIC: 233645.

8.2 CODES, STANDARDS, REGULATIONS, AND PROCEDURES

AP-3.10Q, Rev. 02, ICN 0. *Analyses and Models.* Washington D.C., Washington D.C.: Office of Civilian Radioactive Waste Management. ACC: MOL.20000217.0246.

AP-SI.1Q, Rev. 2, ICN 4. *Software Management.* Washington, D.C.: U.S. Department of Energy, Office of Civilian Radioactive Waste Management. ACC: MOL.20000223.0508.

American Society of Metals (ASM) 1994. "Table 13 Corrosion of AISI-300 Series Stainless Steels in a Marine Atmosphere." *ASM Specialty Handbook, Stainless Steels.* Davis, J.R., ed. Page 150. Materials Park, Ohio: American Society of Metals. TIC: 247111.

ASTM E 112-96. 1996. *Standard Test Methods for Determining Average Grain Size.* West Conshohoken, Pennsylvania: American Society for Testing and Materials. TIC: 247198.

ASTM A 262-98. 1999. *Standard Practices for Detecting Susceptibility to Intergranular Attack in Austenitic Stainless Steels.* West Conshohocken, Pennsylvania: American Society for Testing and Materials. TIC: 246017.

ASTM C 1174-97. 1997. *Standard Practice for Prediction of the Long-Term Behavior of Materials, Including Waste Forms, Used in Engineered Barrier Systems (EBS) for Geological Disposal of High-Level Radioactive Waste.* West Conshohocken, Pennsylvania: American Society for Testing and Materials. TIC: 246015.

ASTM G 1-90 (Reapproved 1999). 1990. *Standard Practice for Preparing, Cleaning, and Evaluating Corrosion Test Specimens.* West Conshohocken, Pennsylvania: American Society for Testing and Materials. TIC: 238771.

ASTM G 108-94 (Reapproved 1999). 1994. *Standard Test Method for Electrochemical Reactivation (EPR) for Detecting Sensitization of AISI Type 304 and 304L Stainless Steels.* West Conshohoken, Pennsylvania: American Society for Testing and Materials. TIC: 247129.

ASTM G 3 - 89 (Reapproved 1999). 1989. *Standard Practice for Conventions Applicable to Electrochemical Measurements in Corrosion Testing.* West Conshohocken, Pennsylvania: American Society for Testing and Materials. TIC: 247076.

ASTM G 5 - 94. *Standard Reference Test Method for Making Potentiostatic and Potentiodynamic Anodic Polarization Measurements.* Philadelphia, Pennsylvania: American Society for Testing and Materials. TIC: 231902.

ASTM G 61-86 (Reapproved 1998). 1987. *Standard Test Method for Conducting Cyclic Potentiodynamic Polarization Measurements for Localized Corrosion Susceptibility of Iron-, Nickel-, or Cobalt-Based Alloys.* West Conshohocken, Pennsylvania: American Society for Testing and Materials. TIC: 246716.

ASTM G1-81. 1987. *Standard Practice for Preparing, Cleaning, and Evaluating Corrosion Test Specimens.* Philadelphia, Pennsylvania: American Society for Testing and Materials. TIC: 246089

ASTM G48-99a. 1999. *Standard Test Methods for Pitting and Crevice Corrosion Resistance of Stainless Steels and Related Alloys by Use of Ferric Chloride Solution.* West Conshohocken, Pennsylvania: American Society for Testing and Materials. Library Tracking Number-L1387.

ASTM G5-87. 1989. *Standard Reference Test Method for Making Potentiostatic and Potentiodynamic Anodic Polarization Measurements.* Philadelphia, Pennsylvania: American Society for Testing and Materials. TIC: 246088.

NRC (U.S. Nuclear Regulatory Commission) 1999. *Issue Resolution Status Report Key Technical Issue: Container Life and Source Term.* Rev. 2. Washington, D.C.: U.S. Nuclear Regulatory Commission. TIC: 245538.

QAP-2-3, Rev. 10. *Classification of Permanent Items.* Las Vegas, Nevada: CRWMS M&O. ACC: MOL.19990316.0006.

QAP-2-0, Rev. 5, ICN 1. *Conduct of Activities.* Las Vegas, Nevada: CRWMS M&O. ACC: MOL.19991109.0221.

UCRL-ID-132285. *Formulation and Make-Up of Simulated Dilute Water, Low Ionic Content Aqueous Solution.* Livermore, California: Lawrence Livermore National Laboratory. TIC: 245767.

UCRL-ID-132286. *Formulation and Make-Up of Simulated Concentrated Water(SCW), High Ionic Content Aqueous Solution.* Livermore, California: Lawrence Livermore National Laboratory. TIC: 245768.

UCRL-ID-132287. *Formulation and Make-Up of Simulated Acidic Concentrated Water (SAW), High Ionic Content Aqueous Solution.* Livermore, California: Lawrence Livermore National Laboratory. TIC: 245766.

YAP-SV.1Q, Rev 0, ICN 1. *Control of the Electronic Management of Data*. Las Vegas, Nevada: Yucca Mountain Site Characterization Project. ACC: MOL.19991008.0209.

8.3 SOURCE DATA

LL991208405924.098. General Corrosion and Localized Corrosion of Waste Package Outer Barrier. Submittal date: 12/20/1999. Submit to RPC

LL991210405924.106. Degradation of Stainless Steel Structural Support for Waste Package. Submittal date: 01/11/2000.